The RESET tephra database and associated analytical tools

Christopher Bronk Ramsey [1,*] Rupert A. Housley [2]
Christine S. Lane [1] Victoria C. Smith [1] A. Mark Pollard [1]

Abstract

An open-access database has been set up to support the research project studying the 'Response of Humans to Abrupt Environmental Transitions' (RESET). The main methodology underlying this project was to use tephra layers to tie together and synchronise the chronologies of stratigraphic records at archaeological and environmental sites. The database has information on occurrences, and chemical compositions, of glass shards from tephra and cryptotephra deposits found across Europe. The data includes both information from the RESET project itself and from the published literature. With over 12,000 major element analyses and over 3000 trace element analyses on glass shards, relevant to 80 late Quaternary eruptions, the RESET project has generated an important archive of data. When added to the published information, the database described here has a total of more than 22,000 major element analyses and nearly 4000 trace element analyses on glass from over 240 eruptions.

In addition to the database and its associated data, new methods of data analysis for assessing correlations have been developed as part of the project. In particular an approach using multi-dimensional kernel density estimates to evaluate the likelihood of tephra compositions matching is described here and tested on data generated as part of the RESET project.

Key words: Dating, Volcanology, Tephra, Statistical methods, Archaeology, Quaternary environments, Cryptotephra, Tephrochronology

* christopher.ramsey@rhala.ox.ac.uk
[1] Research Laboratory for Archaeology, University of Oxford, Dyson Perrins Building, South Parks Road, Oxford, OX1 3QY
[2] Department of Geography, Royal Holloway University of London, Egham, Surrey, TW20 0EX, UK

1 Introduction

The RESET project aimed to use a variety of different methods to achieve the high resolution chronology needed to address questions relating to past rapid climate change, and the human responses to it. The project covers Europe and N. Africa over the time range 10-60 ka BP. However, one of the key elements underpinning the RESET approach has been the construction of a tephrochronological framework, or lattice, which can be used to tie together the chronologies of different types of record at archaeological and palaeoenvironmental (terrestrial and marine) sites. In order to develop this chronostratigraphy, it has been necessary to acquire detailed information about these tephra and cryptotephra deposits, both in terms of their composition and distribution. The RESET database has been an important tool for sharing this information within the group and is now a major resource for other researchers to use.

The database is relational in nature allowing very different types of information to be accessed in a number of different ways. We have included both information generated during the RESET project itself and also information from publications, and gathered in previous data compilations. In addition to the data itself, the database consists of an easily accessible user-interface and a number of geographic, graphic and mathematical tools for data visualisation and analysis. The emphasis here has been on making the data easy to use. The reason for developing a database specifically for this project is that it has enabled the organisational structure to be specifically designed for addressing the project's research aims. The database implementation has also allowed for the integration of tools for data-analysis.

A summary of the data is given in Table 1, showing the scale of data available both from the RESET project and from the published literature, including major inputs from the the Natural Environment Research Council (NERC) QUEST project, and from Felix Riede's compilation of sites where the Laacher See Tephra is found (Riede and Wheeler, 2009; Riede et al., 2011). The term 'Site' includes volcanoes, proximal volcanic sediments and distal locations such as archaeological sites or palaeoenvironmental records. 'Samples' can either be tephra deposits or sediments from archaeological and environmental sites tested for the presence of volcanic glass particles. Where these samples, contain glass shards, they have been analysed for major and trace elements. Usually multiple measurements are made on glass shards from each sample to assess the compositional range. Uncertainties (1σ) on the data presented within the database can be estimated from repeat analyses of the secondary standards analysed with the samples [3]. Sometimes the analyses enable to the glass to be

[3] Using a compilation of secondary standard data run over numerous analytical

	RESET	Other	Total
Sites	185	952	1,152
Samples	5,679	1,817	7,496
Samples with major element analyses of glass	413	689	1,102
Samples with trace element analyses of glass	303	37	340
Major element analyses of glass	12,272	10,435	22,707
Trace element analyses of glass	3,572	421	3,993
Identified volcanic centres	31	26	44
Regional volcanic centres	5	6	6
Total volcanic centres	36	32	50
Eruptions	91	236	284
Eruptions with major element analyses	79	195	240
Eruptions with trace element analyses	67	21	85

Table 1
Summary of the main information in the database as of February 2014. The columns refer to data directly from the RESET project, data from other published sources, and the overall totals. In some instances sites and eruptions are associated with data from both RESET and other published sources.

correlated to particular eruptions or, failing that, to volcanic centres. Some eruptions are known from stratigraphic and compositional analyses of proximal deposits, but other eruptions are only known from distal tephra or cryptotephra deposits and the volcanic source of these may be identified only as a region containing multiple volcanic centres.

Identification of tephra or cryptotephra deposits through major and trace element analyses of associated glass shards is normally done through the visual

sessions we estimated that the errors for each element are: ± 0.6 RSD% for typical SiO_2 concentrations (>50 wt%); ∼ ±1 RSD% for typical Al_2O_2 concentrations (>10 wt%); ∼ ±10 RSD% for Na_2O contents <1 wt% and fall to less than ±5 RSD% when Na_2O contents are >4 wt%; <±2 RSD% at K_2O contents >2 wt%; ±3 RSD% at CaO concentrations of 1.7 wt% and <1.5 RSD% at concentrations >5 wt%; ∼ ±4 RSD% at FeOt (all Fe expressed as FeO) concentrations of ∼3 wt% and <±2 RSD% at >10 wt% FeO; ∼ ±15 RSD% at MgO contents of ∼0.5 wt% and <±2 RSD% at >2 wt%; ∼ ±10 RSD% at TiO_2 concentrations of ∼0.3 wt% and <±2 RSD% at concentrations >2 wt%. Phosphorus, Cl and Mn are typically found in low concentrations, <0.2 wt%, and the errors on these elements are significantly larger. They are around ±40 RSD% for Cl at typical concentrations of ∼0.04 wt%, and ∼ ±30 RSD% for MnO concentrations of ∼0.15 wt%. Errors in P_2O_5 are ∼ ±30 RSD% at 0.1 wt% and drop to <±7 RSD% at concentrations >0.25 wt%.

comparison of analyses on unknown deposits to those on identified eruptions together with stratigraphic, chronological, and mineralogical data that are available.. This visual inspection can be supplemented by statistical analysis using methods such as principle components analysis and discriminant analysis. Because the diagnostic features of the constituents of different tephra or cryptotephra deposits are different for each case, this process tends to be time-consuming and is, by its nature, not quantitative. Here we show that it is possible to use multi-dimensional kernel density estimates to evaluate the likelihood of tephra correlations. An on-line tool has been developed, that enables large numbers of possible source eruptions to be tested rapidly, with quantitative information on the possible identifications. Such statistical methods will not replace detailed consideration of the volcanic systems in question, but they may provide a useful tool in narrowing down possible correlations and help to give better criteria for positive matches.

2 Database structure

The database is divided into a number of related tables. The main tables in the database are:

- *sites/volcanoes*: this table lists all sites within the database, whether they be volcanic centres, or sites of archaeological and environmental interest; each site has associated with it basic information on location (longitude, latitude, altitude, country and region); in the case of volcanic centres the region specified is the volcanic region, which is important in tephra identification (see below); each site can have multiple references associated with it and can also have metadata (text files, plans etc.) with further associated details.
- *samples*: samples within a site can have 3-D coordinate information associated with them; where the sample has tephra or cryptotephra present this is identified as a proximal, mid-distal or distal deposit and the volcanic material type is also specified; except in the case of proximal deposits, a shard count (normally as g^{-1} dry weight but in some cases where comments indicate as cm^{-3}) is given.
- *eruptions*: for each volcanic centre, known eruptions are listed in this table; the eruptions description gives the type of eruption (Plinian, Ultra-Plinian etc.) and the best estimate of the date or age of the eruption with an associated uncertainty and timescale; the reference for the date or age given is also part of the eruption record.
- *identifications*: this is the table which links samples that contain tephra or cryptotephra to individual eruptions, volcanic centres or volcanic regions; in each case a certainty of association is given as a 1-5 scale; the identification is if possible associated with the person who made the identification.
- *instruments*: this is a list of instruments used for analysis of tephra chem-

istry; each instrument record specifies instrument type and location; where the instrument is not known generic instrument types are still specified.
- *batches*: this table lists batches of analyses that have been performed together; this enables measurements on secondary standards (e.g., MPI-DING reference glasses; Jochum et al., 2006) to be linked to the measurements on unknown glass samples to assess analytical accuracy and precision; each batch has information on instrument running parameters and any comments made by the researcher running the analysis; for much published data this information is not available and data are simply grouped by associated publication.
- *majors*: each individual major-element analysis of glass is listed in this table; this is linked to a specific sample from the *samples* table and to a batch in the *batches* table; the unnormalised data is stored in the database but this can be displayed either as normalised or unnormalised; each measurement can have multiple references associated with it where the data are published.
- *trace*: each individual trace-element analysis is listed in this table; this is linked to a specific sample from the *samples* table and to a batch in the *batches* table; each measurement can have multiple references associated with it where the data are published.
- *references*: this table lists the full bibliographic details of all references; this table is linked to sites (multiple references allowed), major/trace element glass analyses (multiple references allowed) and the best-estimate dates or ages for eruptions (one reference allowed).

3 Database implementation

The RESET database uses an open-source MySQL engine and a web interface based on php. The database is available online at `https://c14.arch.ox.ac.uk/resetdb/db.php`. The database is currently read-only for those not involved with the RESET project, though in the future it may be possible for users to add their own data for their own use, and request to have them made publicly available through the database after publication.

3.1 Navigation of the database

Figure 4 shows the front page of the RESET database. There are links here to many of the main aspects of the database, and the menu provides access to the same pages even when the front page is not shown.

The navigation follows logically from the structure of the database laid out above. The principal ways in which the data can be viewed are: by site, by

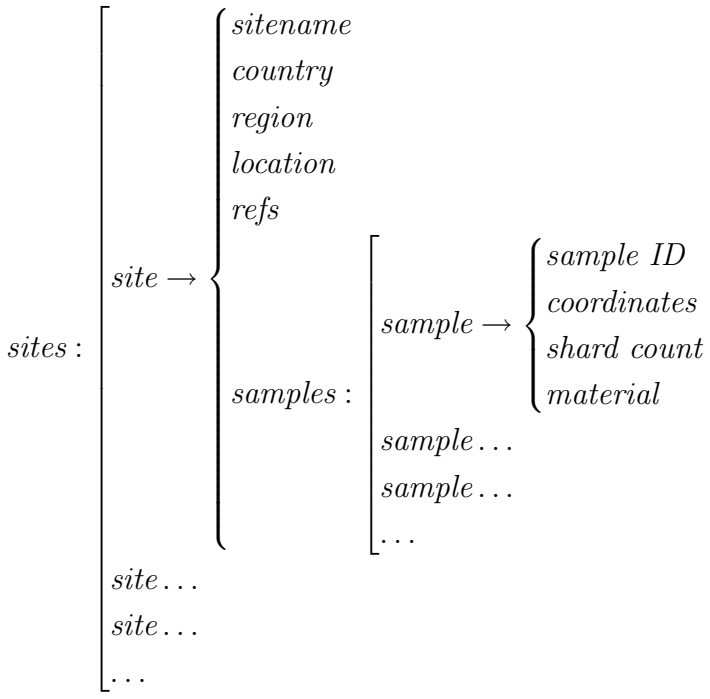

Fig. 1. The main structure of data in the database relating to environmental and archaeological sites. In this figure [brackets denote arrays and { records within the database; the term *refs* refers to a series of references.

volcano or eruption, and by reference. In addition, users can also look at individual batches of analyses by instrument which enables them to find associated measurements on reference standards. All data within the database are hot-linked and so, for example, where a specific eruption is listed in a record, clicking on the eruption name will call up the page that summarises all of the information for that eruption.

Accessing information for individual sites can be done in a number of different ways. If a site location is known, the country can be selected from the page listing all countries for which there are data; the country page shows a list of all sites located within that country, from which a selection can be made. Alternatively, users can generate an alphabetical list of all sites that have samples with information on the database. Finally, sites can also be linked from maps (see below). Any of these means can be used to bring up a site page which lists important information stored on that site in the database (see Figure 5). In addition to a header with information about the sites location, comments and metadata, the site page has four main data-tables: *Samples* which shows samples listed by depth in the site; *Identifications* which are those samples that have been associated with particular eruption events through tephrostratigraphy; *Samples with majors* which lists all glass samples on which chemical analyses have been undertaken (typically those with trace element analyses also have major element analyses); *References* which lists references specific to this site. From this site page users can use the menu item [View >

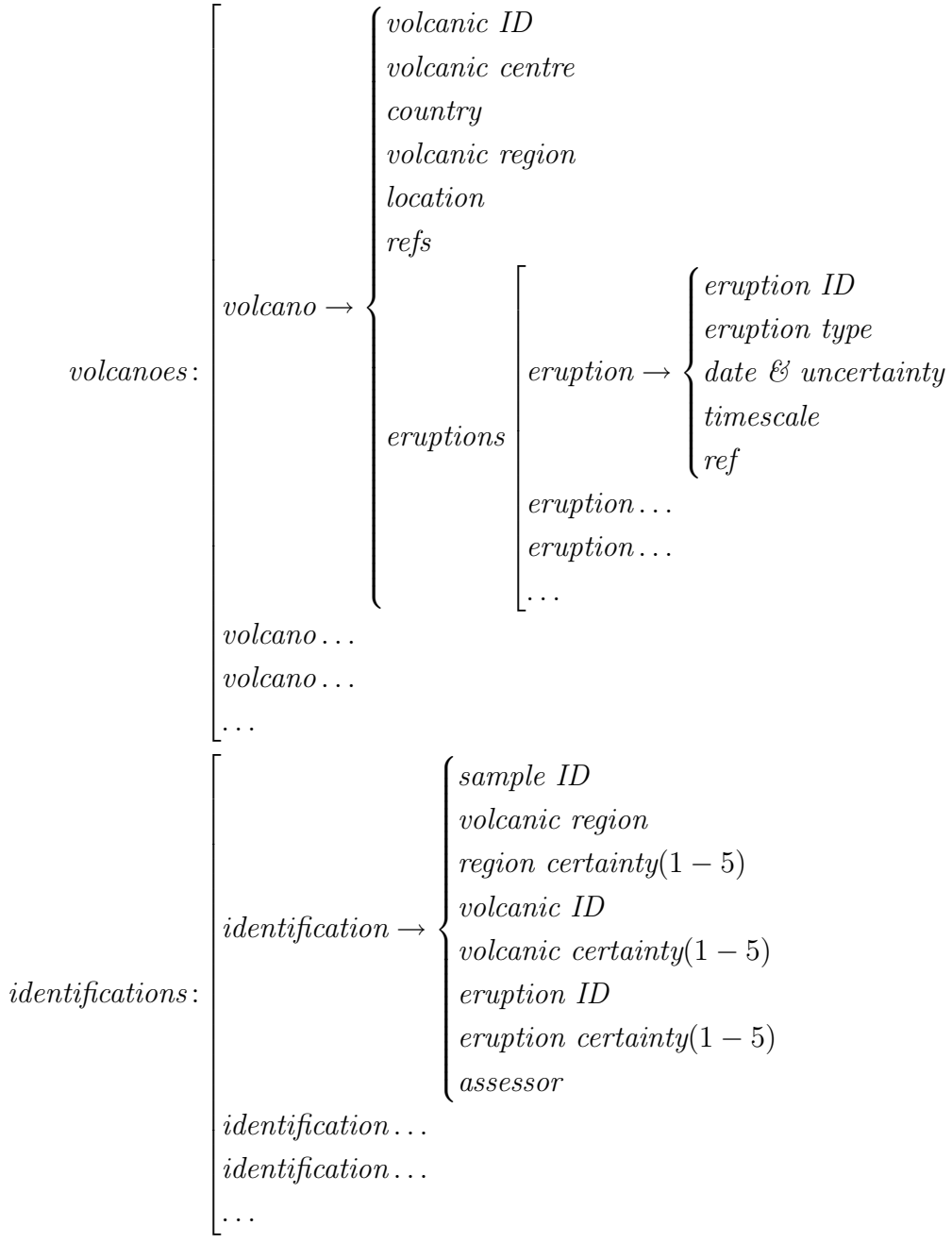

Fig. 2. The main structure of data in the database relating to volcanic centres and associated samples. In this figure [brackets denote arrays and { records within the database; the term *ref* refers to single reference link and *refs* refers to a series of references.

Show on map] to plot the site on a map (see section 3.3) and [View > Plot shard count] will plot the samples from the site by depth (see section 3.2). The same can be done using the plot (✉) and map (🌍) buttons to the right of the menu bar. Pressing the ◁ button returns to a list of all sites in the associated

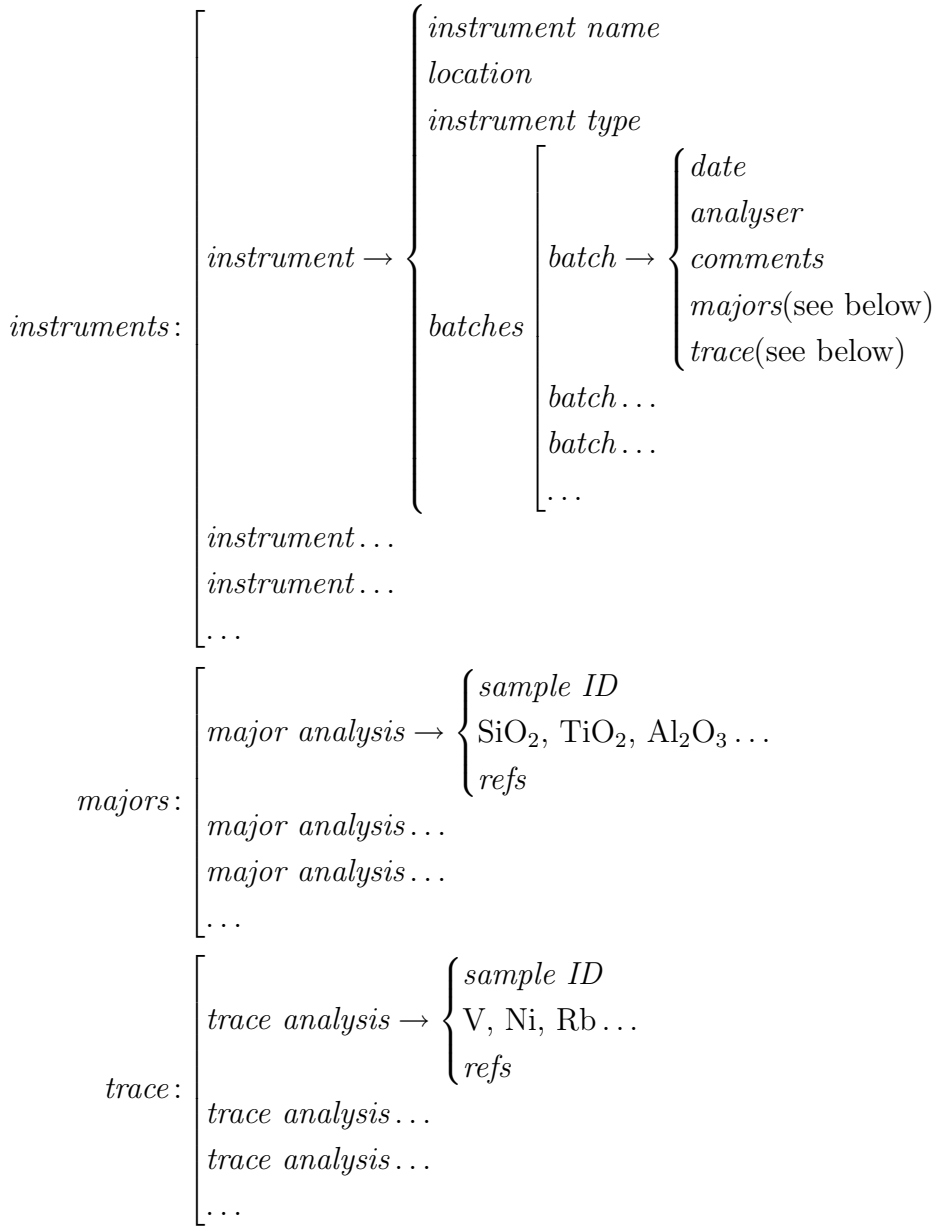

Fig. 3. The main structure of data in the database relating to environmental and archaeological sites. In this figure [brackets denote arrays and { records within the database; the term *refs* refers to a series of references.

country.

A similar approach is taken with volcanic centres and eruptions. The volcanic centre page shows a list of eruptions and all of the associated glass chemical data, whereas the eruption page narrows this information down to the subset of data identified to the specific eruption event. To get to an eruption page, users can either navigate via the volcanic centre, or from the chronological list of all eruptions.

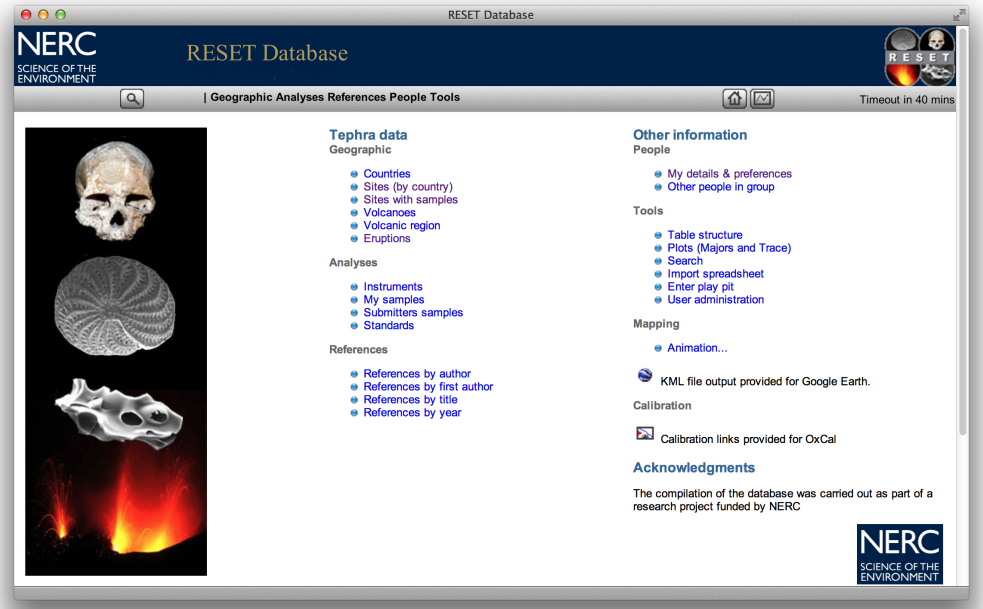

Fig. 4. Home screen of the RESET database.

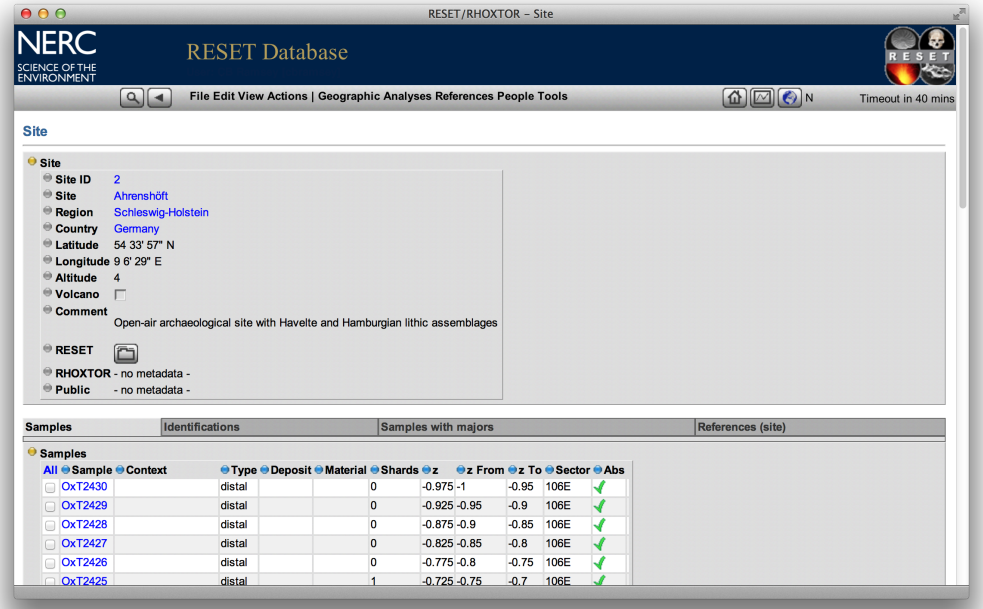

Fig. 5. Site page for the archaeological site of Ahrenshöft, Germany.

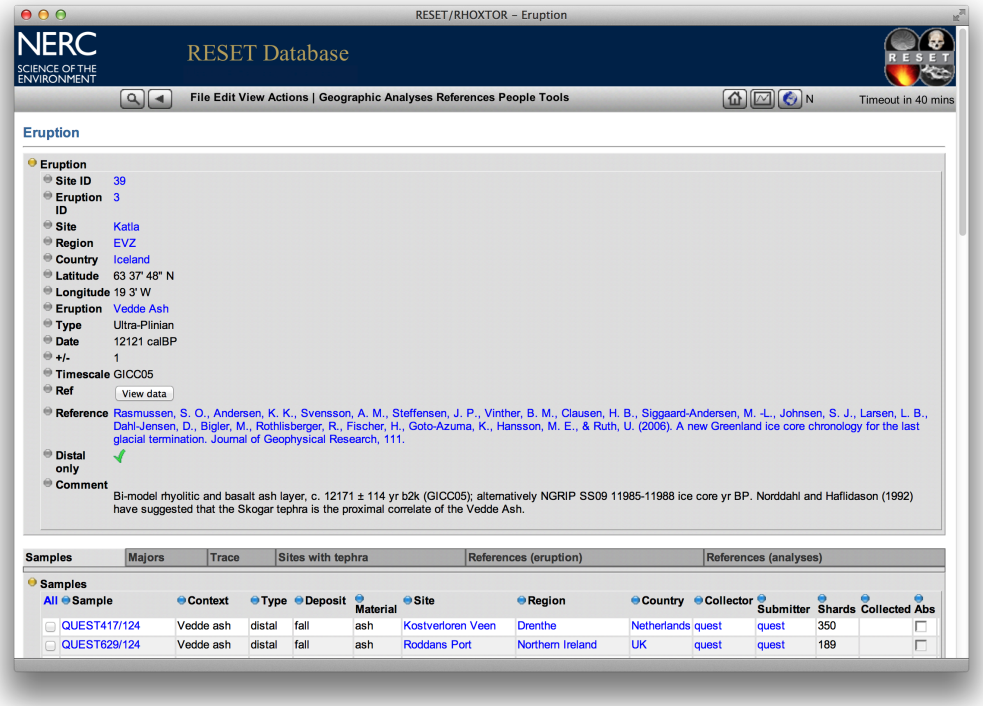

Fig. 6. Eruption page for the widespread Vedde Ash layer from Iceland.

3.2 Plotting data

The database has a built-in plotting facility ('OxPlot') which is able to present the data from the database without exporting to other programs. The purpose of this facility is to enable the rapid visualisation of data from the database, and to simplify the preparation of reports for publication. There are essentially three main type of plots generated by the database: profile plots for cores or sediment sections, glass chemistry plots, and maps (see next section).

Once on a site page (such as Figure 5) within the database, where there are data on samples at different depths, using the [View > Plot shard count] option will produce a plot of the shard count against depth for that site (see Figure 7A). Where there is more than one section or core within the site, within the plotter this detail can be explored by selecting the [View > Multiplot] option (see Figure 7B). This multi plot function provides a useful way to look at the distribution of tephra or cryptotephra at a site.

Probably the most important aspect of the database's plotting functions, however, is the ability to plot glass-shard compositional data and to compare different glass compositions. Any page which contains major or trace element data for glass can be entered into a plot. As a default the database will work with major element data, but trace element plots can also be selected (see

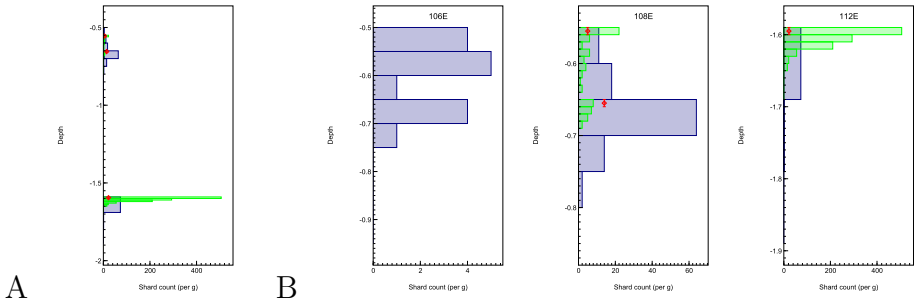

Fig. 7. Shard count plot for the site of Ahrenshöft (Housley et al., 2012). Panel A shows the simple plot against depth (m); panel B shows shard count divided between the three different profiles at this particular site. In each case the blue histogram shows the low resolution scan for glass, and the green histogram the higher resolution scans. The shard counts are given in shards (g^{-1}). The red markers show where samples have been taken for major element analysis (position shown on the y-axis and analysis count on the x-axis).

later in this section). For example, when on the database page for a specific eruption, pressing the plot button at the top right of the page will present the user with a plot of the total alkalis (Na_2O and K_2O) versus SiO_2 (TAS; Le Maitre, 2002, p. 36) for the glass analyses on deposits from that eruption (see, for example, Figure 9). All data from that eruption will be shown. However, this information can also be subdivided: within the plotting routine if [Edit > Import] is selected it is possible to split the data according to different criteria - for example by material or by instrument used for the analysis. By selecting [Edit > Data] (also within the plotting routine) it is possible to select which datasets to put on the plot.

The plotting routine is cumulative and so, once the data for glass from one eruption have been plotted, it is possible to select another eruption in the database and plot the data from analyses of glass for its eruptives alongside. Examples of this kind of plot are shown later in this paper (Figures 13 and 15). In addition, it is possible to import data which is not in the database using the [Edit > Import] function of the plotter (see section 5.1 for an example). This function enables the users to look at their data against reference datasets held in the database.

In addition to the TAS plots, if the user selects [View > Multiplot] from within the plotting routine, a matrix of major element plots is displayed (examples are given in Figures 14 and 16 below).

Finally, to examine the trace element data instead of the major element data, it is necessary to set up an appropriate plot. To do this users can go to the [Tools > Plots] page of the database and select which trace element they wish to plot against (default is Nb). This will set up a blank plot. After navigating to the relevant pages of the database it is then possible to add the data required

to the plot, either using the plot button from the database or using the [Edit > Import] option within the plotter (which allows the data to be split by different criteria).

3.3 Geographical data

The plotting routine associated with the database is also set up to allow the mapping of spatial geographical information. Wherever a page in the database shows location information, this can be mapped either using the internal mapping routine of the database by selecting [View > Show on map] or can be downloaded as KML [4] data by using [View > Download KML].

As an example, if the Laacher See Tephra (LST) is selected in the database, which contains a large collection of occurrences of this tephra, largely from Riede and Wheeler (2009) and Riede et al. (2011), this can be used to generate the map shown in Figure 8. Each point in the map is hot-linked back to the database so that further information can be found. This ability to switch between map and stored information is why the integration of geographic display within the database is so important.

The maps generated can use either the simple coastline underlay shown in Figure 8, or any of the four main Google Map™ views (roadmap, satellite, hybrid or terrain) available from the Google Map™ server. The map underlay can be set from the [Format] menu of the plotting tool. The coastline outline is a Scalable Vector Graphics (SVG), public domain map and is more suitable for publications.

3.4 Technical details

The php code used for extraction of data from the database is fairly simple: its function is primarily to allow secure access to the data and to perform the SQL searches on the database. The data from the database are then sent to the user as javascript arrays and objects. All of the presentation and numerical analysis of the data takes place on the clients machine within the javascript engine of the user's browser. This approach has two main advantages: data only have to be retrieved once because data comparison and presentation do not require extra searches to be performed on the database, minimising the effect of low connection speeds; furthermore the server itself does not have to prepare data for presentation or do any numerical analysis, which improves performance of

[4] Keyhole Markup Language (KML) is an XML format for geographic information developed for Google Earth™

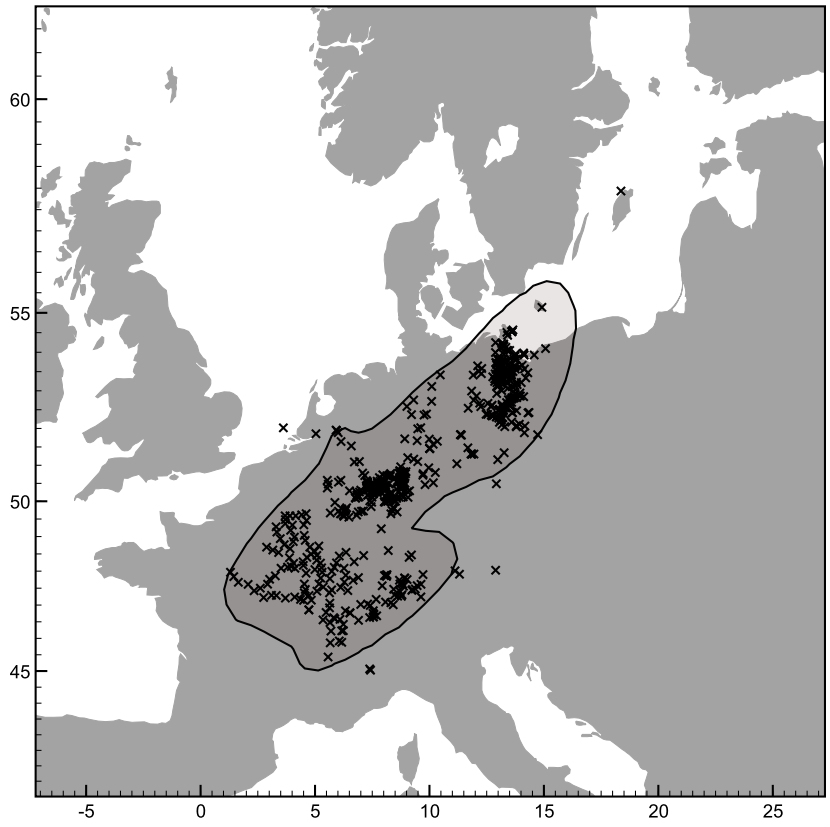

Fig. 8. Distribution of occurences of the LST with information stored in the database. The grey outline shown is a 95% contour of a kernel density generated from the mapped points. It shows the approximate main extent of find sites (which not necessarily the same as the original tephra distribution).

the system with multiple users. However, there are also some disadvantages to this approach: the quantity of data being analysed can be quite high and client computers without much memory, or with low performance web-browsers, may find that the system is slow to use, or cannot cope if they try to retrieve and plot data on analyses of glass shards from a very large number of different eruptions.

To see how the database methodology works in practice, users can navigate to a site page such as that shown in Figure 5 and look at the page source. Here they will see the raw data extracted from the database as a javascript data object.

The statistical comparison tool is all written in javascript and is therefore openly available. The main comparison routines are all given in one file `https://c14.arch.ox.ac.uk/utils/kde.js`

The graphics generated by the database are also generated dynamically within the web-browser of the user. This has the advantage that these processor intensive tasks do not slow down the server. The graphics use the SVG standard, compatible with most of the latest generation web-browsers. The plots generated can be saved in this format (editable with the open source Inkscape package or various commercial alternatives such as Adobe™ Illustrator) or can be converted to pdf or png format using Apache™ Batik toolkit installed on the server.

4 Statistical comparison tools

Comparing datasets from analyses of glass derived from tephra or cryptotephra deposits raises issues common to many multivariate datasets. In this case there are reference datasets (which are known to be associated with particular eruptions for example) and candidate datasets which are to be tested against the references. The problem becomes two-fold: how the reference dataset be summarised and how can matches be tested. The first of these problems is complicated by the fact that distributions of chemical data from glass are often not well approximated by a multivariate normal distribution and in particular can be multi-modal. Two options are considered here: using multivariate normal distributions and kernel density distributions. Both methods use unnormalised data.

In each case the reference dataset $\boldsymbol{X}$ is assumed to comprise n measurements, each with d parameters:

$$\boldsymbol{X} = \begin{pmatrix} x_{11} & x_{12} & \dots & x_{1d} \\ x_{21} & x_{22} & \dots & x_{2d} \\ \vdots & \vdots & \ddots & \vdots \\ x_{n1} & x_{n2} & \dots & x_{nd} \end{pmatrix} = \begin{pmatrix} \boldsymbol{x}_1 \\ \boldsymbol{x}_2 \\ \vdots \\ \boldsymbol{x}_n \end{pmatrix} \tag{1}$$

A candidate distribution $\boldsymbol{Y}$ will be defined in the same way but with m measurements, each with d parameters. In other words, it is assumed that for any comparison the same parameters are measured on the reference and candidate datasets (or that any measurements not made on both datasets are ignored).

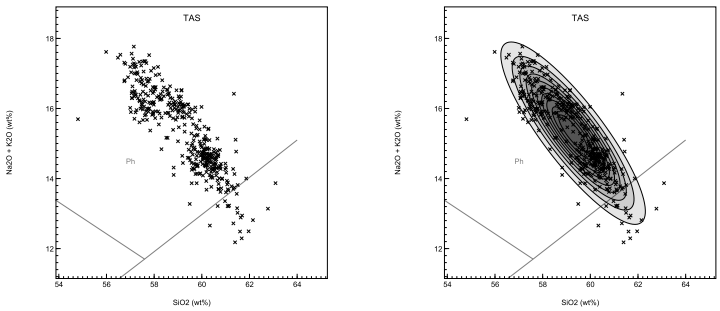

Fig. 9. Major element data for glass shards from the Laacher See Tephra plotted on a TAS plot (normalised data displayed); the plot on the left shows the individual data points and that on the left shows the multivariate normal distribution derived from these.

4.1 Multivariate normal distribution

A multivariate (n dimensions) dataset can be summarised by its mean $\boldsymbol{\mu}$ and covariance $\boldsymbol{\Sigma}$ where:

$$\boldsymbol{\mu_X} = [\mu_1, \mu_2, \ldots, \mu_d] \tag{2}$$
$$\boldsymbol{\Sigma_X} = [\Sigma_{ij}], i = 1, 2, \ldots, d; j = 1, 2, \ldots, d \tag{3}$$

On the assumption that the dataset is drawn from a multivariate normal distribution, the estimate for the probability of any individual point within this distribution will be given by:

$$p_{\boldsymbol{X}}(\boldsymbol{x}) = p_{\boldsymbol{X}}(x_1, \ldots, x_d) = \mathcal{N}_d(\boldsymbol{\mu_X}, \boldsymbol{\Sigma_X}) \tag{4}$$

This can be illustrated using the example of tephra analyses for the Laacher See Tephra (Turney et al., 2006; Finsinger et al., 2008; Riede et al., 2011; Lane et al., 2011b, 2012b; Housley et al., 2013). Figure 9 shows the major element data of glass from the LST plotted on a TAS plot (Le Maitre, 2002) and the associated multivariate normal distribution (10 contours). This simple example shows the limitations of using a multivariate normal model for this type of data in that the peak of the distribution is actually in a composition region which is relatively unlikely.

So if there is another glass shard with measurements $\boldsymbol{y}$ on the same set of parameters, the probability that we would have got these measurements, had the particle come from the same dataset as X, is given by:

$$p_{\boldsymbol{X}}(\boldsymbol{y}) = p_{\boldsymbol{X}}(y_1, \ldots, y_d) = \mathcal{N}_d(\boldsymbol{\mu_X}, \boldsymbol{\Sigma_X}) \tag{5}$$

For a full set of measurements Y, the average value for this probability is:

$$\overline{p_{\boldsymbol{X}}}(\boldsymbol{Y}) = \frac{1}{m}\sum_{i=1}^{m} p_{\boldsymbol{X}}(\boldsymbol{y}_i) \tag{6}$$

Now the absolute value of this average will depend on the normalisation of the chosen parameters. However, the higher this value is the more likely it is that the dataset Y is actually just a subset of that for X. However, it is useful to divide this average value by a similar average for the reference dataset to get a ratio:

$$A_{\boldsymbol{YX}} = \frac{\overline{p_{\boldsymbol{X}}}(\boldsymbol{Y})}{\overline{p_{\boldsymbol{X}}}(\boldsymbol{X})} \tag{7}$$

This value should be close to 1 if the distributions are very similar. It could be greater than 1 if all the measurements in dataset Y cluster in the peak of the distribution X. This ratio is a useful measure because it provides an indication of the degree of overlap between the two distributions. Note that the definition here is not symmetrical (that is $A_{\boldsymbol{YX}} \neq A_{\boldsymbol{XY}}$) because the measure is for $\boldsymbol{Y}$ being a subset of $\boldsymbol{X}$. Now with multiple datasets it is possible to form a matrix of such ratios which can be used to indicate possible matches of unknown (uncorrelated) tephra or cryptotephra to known one. Before looking at this in more detail, the Kernel-density approach will be considered.

4.2 Kernel-density distribution

Kernel density methods have been found useful in a range of applications associated with chemical compositions and geographical distributions (Aitchison and Lauder, 1985; Baxter et al., 1997; Santos et al., 2006; Weller et al., 2006). With multiple dimensions, there is no well-defined method that can be used to estimate the optimal kernel bandwidth. There are various methods which require iterative or MCMS optimisation, sometimes within a Bayesian framework (see, for example, Zhang et al., 2006, for a discussion) but these are by their nature difficult to use in rapid comparison of data. An alternative is to use a commonly applied approximation, which is shown to be approximately optimal in cases which approach normality. To use this the data for any specific dataset, the data are first sphered (using the inverse of the covariance matrix to perform the transformation $x \rightarrow x'$) so that they have variance of one in each dimension. The optimal bandwidth h for the multidimensional spherically symmetric multivariate normal kernels within this space can then be approximated (see Scott (1992) and Bowman and Azzalini (1997) as discussed in Zhang et al. (2006)) by:

$$h = \left\{ \frac{4}{(d+2)n} \right\}^{1/(d+4)} \tag{8}$$

where d is the number of dimensions (different variables) and n is the number of samples. So within this transformed space each kernel takes the form of:

$$\sim \mathcal{N}_d(\boldsymbol{x}'_i, h^2 \boldsymbol{I}) \tag{9}$$

and the overall kernel density distribution is:

$$\sim \frac{1}{n} \sum_{i=0}^{n} \mathcal{N}_d(\boldsymbol{x}'_i, h^2 \boldsymbol{I}) \tag{10}$$

Transforming the data back to their usual multivariate space means that the kernel distributions are skewed in the direction of the covariance seen in the particular dataset. This effect will be apparent through the practical examples given later in this paper. The overall kernel density becomes:

$$q_{\boldsymbol{X}}(\boldsymbol{x}) = q_{\boldsymbol{X}}(x_1, \ldots, x_d) = \frac{1}{n} \sum_{i=0}^{n} \mathcal{N}_d(\boldsymbol{x}_i, h^2 \boldsymbol{\Sigma}_{\boldsymbol{X}}) \tag{11}$$

Figure 10 shows the major element data for the LST plotted on a TAS plot (compare to Figure 9), in this case just using two dimensions. The kernel density approach gives a better representation of the underlying distribution.

The aim is to use these improved distributions to test for matches in much the same way that the multivariate normal distributions were used above. Here, however, there is a slight complication when normalising in that if we calculate $\overline{q_{\boldsymbol{X}}}(\boldsymbol{X})$ we might expect to get an artificially high value since the data points themselves define the peaks of the kernels. To overcome this we miss out the kernel associated with the test point while performing the sum. Using the modified distribution:

$$q_{\boldsymbol{X}\bar{j}}(\boldsymbol{x}) = \frac{1}{n-1} \sum_{i=0, i\neq j}^{n} \mathcal{N}_d(\boldsymbol{x}_i, h^2 \boldsymbol{\Sigma}_{\boldsymbol{X}}) \tag{12}$$

the appropriate data comparison matrix (where $\boldsymbol{X} \neq \boldsymbol{Y}$) becomes:

$$B_{\boldsymbol{Y}\boldsymbol{X}} = \frac{\frac{1}{m} \sum_{i=0}^{n} q_{\boldsymbol{X}}(\boldsymbol{y}_i)}{\frac{1}{n} \sum_{j=0}^{n} q_{\boldsymbol{X}\bar{j}}(\boldsymbol{x}_j)} \tag{13}$$

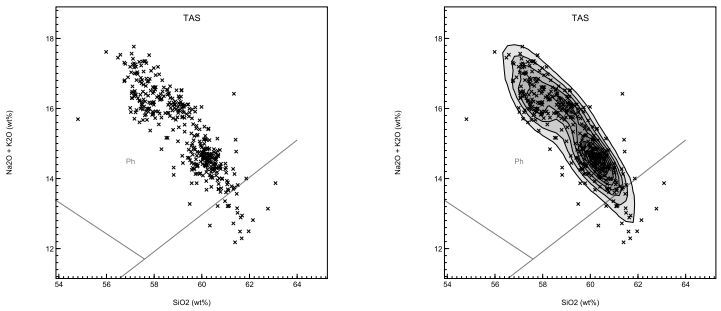

Fig. 10. Major element data for glass from the Laacher See Tephra plotted on a TAS plot (normalised data displayed); the plot on the left shows the individual data points and that on the left shows the kernel density estimate distribution derived from these datapoints; this plot should be compared to Figure 9.

and $B_{\boldsymbol{XX}} \equiv 1$.

4.3 Significance of comparisons

Whenever comparing chemical datasets, it is impossible to prove that two datasets are the same. Logically, it is only possible to show that two datasets are *unlikely* to be the same. For this reason it is suggested that the matrix elements $A_{\boldsymbol{YX}}$ and $B_{\boldsymbol{YX}}$ be used to indicate where it is unlikely that dataset $\boldsymbol{Y}$ is a subset of dataset $\boldsymbol{X}$. Any threshold that is chosen will be arbitrary but anything lower than 0.05 indicates that the average probability for the points measured is below 5% of the expected value, and this is a good working value. The examples below will show how this works in practice.

4.4 Implementation of the statistical tools

The statistical tools used in this database are integrated into the plotting package ('OxPlot') linked to the database. There are three tools specifically included which can be accessed from the [Tools] menu item of the plotter.

- *PCA*: This performs a principle components analysis (PCA) of the datasets imported into the plotter. Users is prompted for which variables they wish to include (e.g., SiO_2, Al_2O_3, CaO). Running the analysis will generate the PCA matrix and λ values for each component. This matrix can be exported to a spreadsheet. In addition, running this analysis sets up a plot of the data against the two principal components (PC1 and PC2).
- *Ellipsoid matrix*: This will calculate the matrix $A_{\boldsymbol{YX}}$ based on multivariate normal distributions as described above. The matrix generated can be exported to a spreadsheet.

- *KDE matrix*: This will calculates the matrix $B_{\boldsymbol{YX}}$ based on kernel density analysis as described above. The matrix can be exported to a spreadsheet.

In addition to the formal tools, the plotting routine also uses the same mathematical formalism for another purpose. For each dataset plotted it is possible to show either a multivariate normal distribution or a kernel density distribution (based on normalised or unnormalised data, depending on the user's choice). In both cases the distribution can be represented either by a series of contours (5, 10 or 20 levels) or as a single 95% probability contour (these options are set under the [Format] menu. In the case of multivariate normal distributions the software puts an ellipse around the datasets, the kernel density method puts a more free-form curve around the data. There is a convenient way to turn this form of display on and off for all datasets using [View > Toggle ellipses] and [View > Toggle KDE]. Control of what is displayed for each dataset is given under the [Edit > Data] option.

5 Example applications

In this section two different applications of the database will be examined which are chosen to illustrate its utility. The first case study shows the way in which the database can be used to help with the study of deposits at a particular site. In this case the data are from cryptotephra and tephra deposits found in the sediments of Soppensee (Lane et al., 2011b, 2012a). The second case study will focus on the use of the database and the comparison tools to summarise information about all of the tephras and cryptotephras in the RESET tephra lattice.

5.1 Identification of tephra from Soppensee

The background to this study is presented in Lane et al. (2011b), with relevant further discussion in Lane et al. (2012a). There are four deposits where there are tephra-derived glass shards present: two are visible (Sop_T4.74 and Sop_T5.95) and two are cryptotephra concentrations (Sop_T5.19 and Sop_T5.62). The data for this case study are given in the supplementary online information, organised into a table suitable for import into the plotting routine.

To use the database for an exercise like this, a blank TAS plot can be generated from the database. Using the [Edit > Import] function of the plotter, the data can then be pasted into the the plotter, and split by tephra/cryptotephra deposit to give separate datasets for each deposit. From the database users can then select glass-shard data from eruptives that are possible correlates with

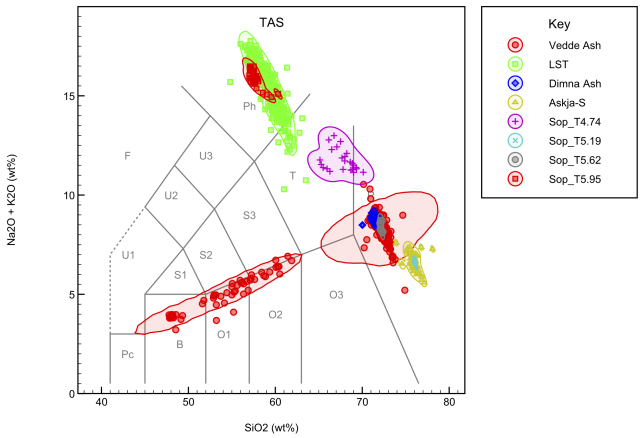

Fig. 11. Major element data for glass shards from tephra/cryptotephra deposits from Soppensee plotted on a TAS plot with 95% KDE contours (See Le Maitre, 2002, for field key; data nomalised). This provides an immediate indication of the most likely identifications for the different deposits. However, it can be seen that Sop_T5.62 could either be correlated with the Vedde or the Dimna Ash and it is not immediately obvious which one is most likely. An aspect of the KDE implementation is also visible here, shown by the Vedde ash data, which are highly bimodal; the KDE contours are extended in the direction of the mixing line due to non-optimal kernel choice (see section 4.2); this may not look ideal but in practice it means that the KDE matrix will give higher values on a mixing line, even if no points are present, than would be the case if the kernel choice was technically better.

the glass data for the unknown deposits. In this case the Vedde Ash (Birks et al., 1996; Björck and Wastegård, 1999; Blockley et al., 2007; Davies et al., 2001, 2005; Lane et al., 2012a,b; Lowe and Turney, 1997; Matthews et al., 2011; Pilcher et al., 2005; Ranner et al., 2005; Schoning et al., 2001; Turney et al., 1997, 2001, 2006; Wastegård et al., 1998, 2000), LST (Riede et al., 2011; Turney et al., 2006; Finsinger et al., 2008; Lane et al., 2012b; Housley et al., 2013), Dimna Ash (Lane et al., 2012a), and the Askja-S (Davies et al., 2003; Turney et al., 2006; Pilcher et al., 2005; Lane et al., 2012b; Lind and Wastegård, 2011) tephra deposits were chosen. These are added to the same plot using the plot button from the database. This gives the data as shown in Figure 11. It is possible to plot the data for all of the other major elements by selecting [View > Multiplot].

Although such plots are useful for looking at the data, we would prefer to quantify the possible matches. To do this we use the [Tools > Ellipsoid Matrix] or [Tools > KDE Matrix] options. After choosing to use all the major element data this gives us matrices that describe the possible matches available (Tables 2 and 3).

Either of these approaches give us a summary of what all of the different major element glass-shard data tell us of possible matches. In practice the two different methods give similar results, which in some ways in encouraging

Datasets	A	B	C	D	E	F	G	H
A - Vedde Ash	1.000	0.002	**0.077**	0.000	0.000	0.000	0.006	0.000
B - LST	0.000	1.000	0.000	0.000	0.000	0.000	0.000	0.000
C - Dimna Ash	1.054	0.000	1.000	0.000	0.000	0.000	0.000	0.000
D - Askja-S	0.000	0.000	0.000	1.000	0.000	0.000	0.000	0.000
E - Sop_T4.74	0.000	0.000	0.000	0.000	1.000	0.000	0.000	0.000
F - Sop_T5.19	0.000	0.000	0.000	**0.787**	0.000	1.000	0.000	0.000
G - Sop_T5.62	1.156	0.000	0.047	0.000	0.000	0.000	1.000	0.000
H - Sop_T5.95	0.000	0.046	0.000	0.000	0.000	0.000	0.000	1.000

Table 2
Matrix $\boldsymbol{A_{YX}}$ based on multivatiate normal probability distributions (SiO_2, TiO_2, Al_2O_3, FeOt, MnO, MgO, CaO, Na_2O, K_2O) for glass from the tephra and cryptoephra deposits found in Soppensee, and for glass from tephras which might be possible matches

Datasets	A	B	C	D	E	F	G	H
A - Vedde Ash	1.000	0.002	**0.104**	0.000	0.000	0.000	0.030	0.000
B - LST	0.000	1.000	0.000	0.000	0.000	0.000	0.000	0.000
C - Dimna Ash	1.301	0.000	1.000	0.000	0.000	0.000	0.000	0.000
D - Askja-S	0.000	0.000	0.000	1.000	0.000	0.000	0.000	0.000
E - Sop_T4.74	0.000	0.000	0.000	0.000	1.000	0.000	0.000	0.000
F - Sop_T5.19	0.000	0.000	0.000	**0.592**	0.000	1.000	0.000	0.000
G - Sop_T5.62	1.239	0.000	**0.100**	0.000	0.000	0.000	1.000	0.000
H - Sop_T5.95	0.000	0.028	0.000	0.000	0.000	0.000	0.000	1.000

Table 3
Matrix $\boldsymbol{B_{YX}}$ based on KDE probability distributions (SiO_2, TiO_2, Al_2O_3, FeOt, MnO, MgO, CaO, Na_2O, K_2O)

as it implies that the matrix method is not too dependent on the method used to generate the distribution. In both cases there is no match for Sop_T4.74. In fact this visible tephra is thought to be the Vasset Killian tephra from the Massif Central (for which there were no data in the database). Sop_T5.19, also manifest as a visible tephra layer, can clearly be correlated with the Askja 10-ka tephra. Sop_T5.62 (a cryptotephra) matches better with the Vedde than with the Dimna Ash (by a factor of 25 by the multivariate normal method and by a factor of 12 by the more robust KDE method) which is a useful finding. In these three cases the tools provided do seem to do what was intended. The numbers show that the method is asymmetrical and show, for example, that Sop_T5.19 is very likely to be a subset of Askja S but the Askja-S tephra would not be likely to be a subset of a tephra fully represented by Sop_T5.19. This makes sense and shows that the approach can achieve something which statistical distance methods could not.

However, where the method appears not to work so well is with the tephra layer Sop_T5.95, because both methods show a possible weak link to the LST (slightly weaker with the KDE method). However, it is thought that this visible tephra almost certainly is the LST. It is worth considering the reasons for this weakness in KDE correlation in more detail. To do this the other tools within the plotter can be used. Selecting out just the data for the LST and Sop_T5.95, a principal components analysis can be performed, and a plot of the data with KDE contours generated (Figure 12). Here the reason for the poor match can

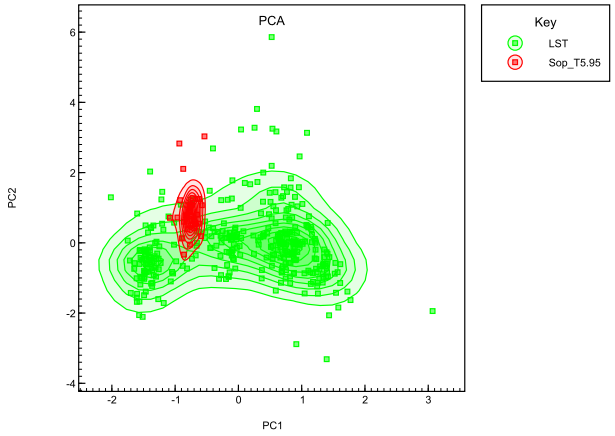

Fig. 12. Principal components analysis of tephra from the LST with that from the Sop_T5.95 layer in Soppensee, which is thought to come from the same eruption. The Sop_T5.95 compositions fall in a low-point in the multimodal distribution from the LST and therefore only provide a weak statistical match. However this is most likely because the LST data in the database is not representative of the compositional range of the entire eruption deposits.

be seen: the data from Sop_T5.95 occupy a space not populated by the LST dataset, even though they do lie within the overall envelope. Presumably this is because the reference dataset is not yet fully representative of all compositions from the eruption. In this case, although the tools have not done exactly what was intended in finding a match, they have helped to explore the differences between the datasets.

5.2 Glass from the RESET tephra lattice

The second application of the comparison tools is to use them to look at a large dataset of glass-shard compositional data found in the database. The tephras chosen are the late Quaternary layers discussed in Bronk Ramsey et al. (2014b). Because glass compositions of tephras or cryptotephras from the Northern and Western European volcanic centres (Iceland, France and Germany) will be easily distinguished from those of Southern Europe, the tephras are split into two groups; this will just have the effect of making the matrices generated easier to display. In practice, the mathematical operations are sufficiently fast that analsyes of glass shards from large number of different tephras can be investigated at the same time.

The selected tephra layers generated from Northern and Western European centres (including Iceland), with major element data, are: Saksunarvatn (Wastegård et al., 2001; Dugmore and Newton, 1997; Andrews et al., 2002; Pyne-O'Donnell, 2007; Birks et al., 1996; Lind and Wastegård, 2011; Bramham-Law et al.,

Datasets	A	B	C	D	E	F	G
A - Saksunarvatn	1.000	0.000	0.000	0.000	0.000	0.000	0.000
B - Askja-S	0.000	1.000	0.000	0.000	0.000	0.000	0.000
C - AF555	0.000	0.000	1.000	**0.607**	0.000	0.000	0.000
D - Vedde Ash	0.000	0.000	0.000	1.000	0.002	0.000	0.000
E - LST	0.000	0.000	0.000	0.000	1.000	0.000	0.000
F - Penifiler Tephra	0.000	0.000	0.000	0.000	0.000	1.000	**0.602**
G - Borrobol	0.000	0.000	0.000	0.000	0.000	**0.673**	1.000

Table 4
Matrix $\boldsymbol{A_{YX}}$ based on multivatiate normal probability distributions (SiO_2, TiO_2, Al_2O_3, FeOt, MnO, MgO, CaO, Na_2O, K_2O) for tephra from Northern and Western Europe which are important in the RESET tephra lattice

Datasets	A	B	C	D	E	F	G
A - Saksunarvatn	1.000	0.000	0.000	0.001	0.000	0.000	0.000
B - Askja-S	0.000	1.000	0.000	0.000	0.000	0.000	0.000
C - AF555	0.000	0.000	1.000	**0.498**	0.000	0.000	0.000
D - Vedde Ash	0.000	0.000	0.000	1.000	0.002	0.000	0.000
E - LST	0.000	0.000	0.000	0.000	1.000	0.000	0.000
F - Penifiler Tephra	0.000	0.000	0.000	0.000	0.000	1.000	**0.650**
G - Borrobol	0.000	0.000	0.000	0.000	0.000	**0.601**	1.000

Table 5
Matrix $\boldsymbol{B_{YX}}$ based on KDE probability distributions (SiO_2, TiO_2, Al_2O_3, FeOt, MnO, MgO, CaO, Na_2O, K_2O) for tephra from Northern and Western Europe which are important in the RESET tephra lattice

2013), Askja-S (Davies et al., 2003; Lane et al., 2011b, 2012b; Lind and Wastegård, 2011; Pilcher et al., 2005; Turney et al., 2006), Abernethy AF555 (Matthews et al., 2011), Vedde Ash (Birks et al., 1996; Björck and Wastegård, 1999; Blockley et al., 2007; Davies et al., 2001, 2005; Lane et al., 2011a,c,b, 2012a,b; Lowe and Turney, 1997; Matthews et al., 2011; Pilcher et al., 2005; Ranner et al., 2005; Schoning et al., 2001; Turney et al., 1997, 2001, 2006; Wastegård et al., 1998, 2000), LST (Riede et al., 2011; Lane et al., 2011b, 2012b; Turney et al., 2006; Finsinger et al., 2008; Housley et al., 2013), Penifiler (Matthews et al. (2011); Pyne-O'Donnell (2007); Pyne-O'Donnell et al. (2008), and originally identified as the Borrobol in Davies et al. (2003)) and Borrobol (Matthews et al., 2011; Pyne-O'Donnell, 2007; Ranner et al., 2005; Turney et al., 1997, 2001). A combined TAS plot for glass-shard analyses from these tephras is shown in Figure 13, with details of the major element compositions shown in Figure 14. Although such plots can be somewhat confusing, with the danger of glass data from different eruptives plotting over one another, because they can be quickly generated from the database, they do provide a way to visualise the spread of glass compositions for a whole region.

As with the case of the single site study for Soppensee, the multivariate normal and KDE matrices can be used to see which glass analyses overlap in the multidimensional space defined by the major element compositions. As with the single site example it turns out that the two different approaches (matrices $\boldsymbol{A}$ shown in Table 4 and $\boldsymbol{B}$ in Table 5) yield very similar conclusions. As an example, AF555 might be mistaken for the Vedde Ash (or indeed for several other minor related tephra from that period that probably all share the

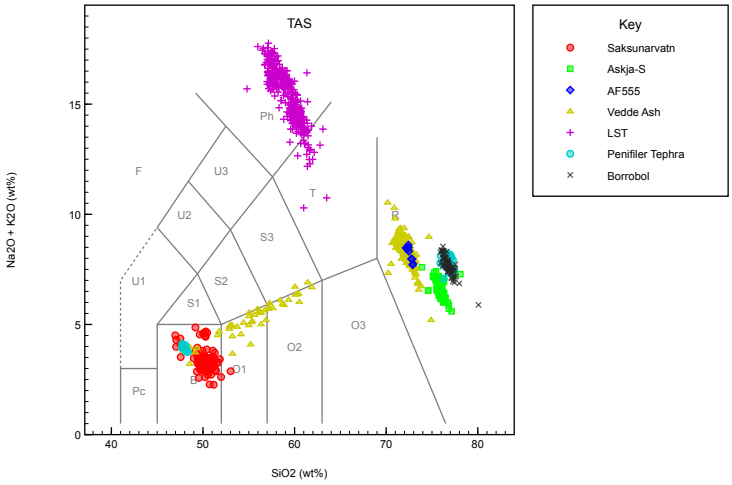

Fig. 13. TAS plot (normalised) for glass shard analyses for tephra/cryptotephra deposits from Northern and Western European volcanic centres which are components of the RESET tephra lattice (Bronk Ramsey et al., 2014b).

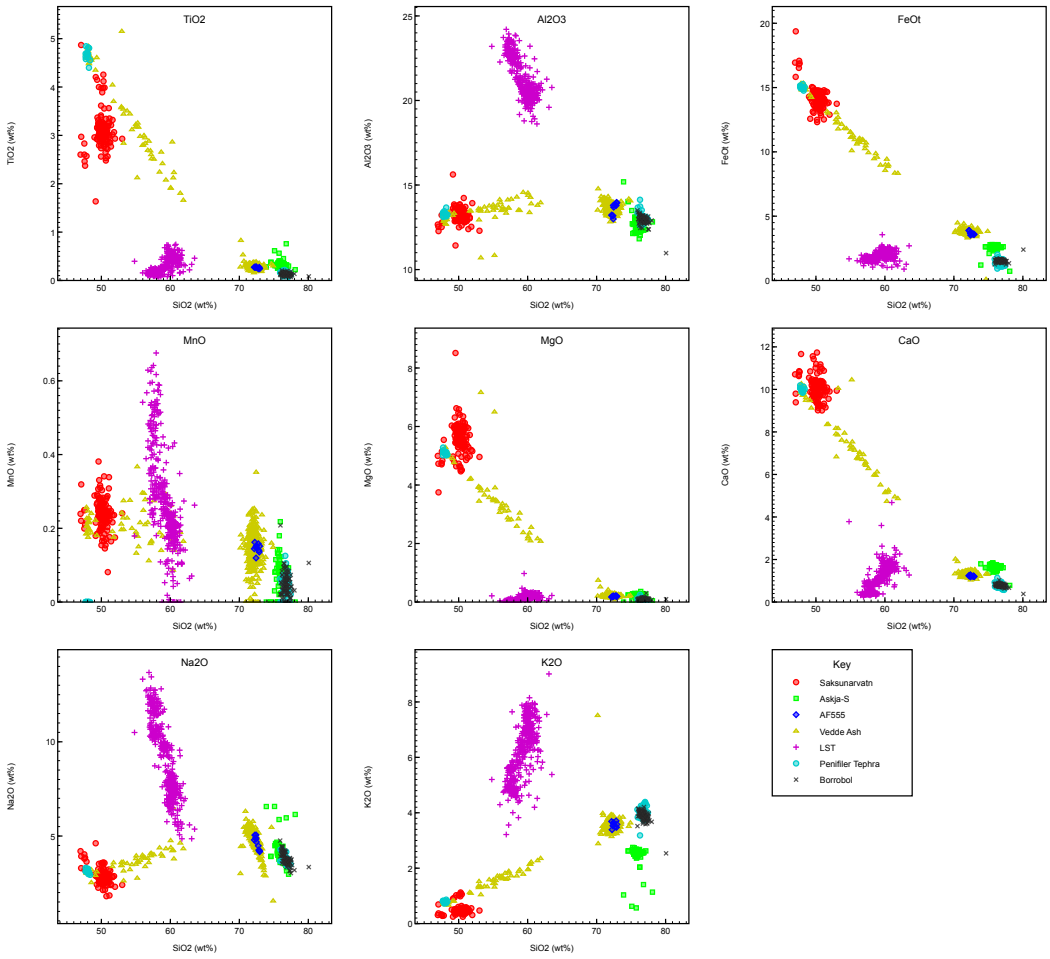

Fig. 14. Major element plots (normalised) for glass shard analyses for tephra/cryptotephra deposits from Northern and Western Europe (c.f. Figure 13).

same source), but it is very unlikely that the Vedde Ash would be mistaken for AF555, from the numerical analysis given here. Of course this conclusion needs to be treated with some caution: this could, for example, be partly because only have a small subset of the original AF555 tephra is present in the distal samples. Chemical data must clearly alway only be considered alongside stratigraphic information.

The next task is to look at the much larger number of tephras layers in this selection from sources in the Mediterranean region. Here we have major element data for glass shards from Pomici Principali (Lane et al., 2011a; Lowe et al., 2007; Magny et al., 2006; Smith et al., 2011; Tomlinson et al., 2012a; Wulf et al., 2004, 2007), Soccavo 1(Smith et al., 2011; Albert et al., 2012), Neapolitan Yellow Tuff (NYT; Bourne et al., 2010; Lane et al., 2011a; Magny et al., 2006; Tomlinson et al., 2012a; Wulf et al., 2004, 2007), Biancavilla-Montalto Ignimbrite (Y1; Douka et al., 2014), TM11 (Wulf et al., 2004, 2007), Verdoline (Wulf et al., 2004, 2007; Bourne et al., 2010; Tomlinson et al., 2014a), Cape Riva (Y2; Wulf et al., 2002; Margari et al., 2007; Kwiecien et al., 2008), Pomici di Base (Wulf et al., 2004, 2007), Y3 (Wulf et al., 2004, 2007; Bourne et al., 2010; Vogel et al., 2009; Tomlinson et al., 2012a), Codola (Bourne et al., 2010; Wulf et al., 2004, 2007; Vogel et al., 2009; Tomlinson et al., 2014a), Campanian Ignimbrite (Y5, C13; Bourne et al., 2010; Douka et al., 2014; Margari et al., 2007; Morley and Woodward, 2011; Pyle et al., 2006; Seymour and Christanis, 1995; Tomlinson et al., 2012a; Vogel et al., 2009; Wulf et al., 2004, 2007), Green Tuff (Y6; Vogel et al., 2009), Nisyros Upper Pumice (Margari et al., 2007; Tomlinson et al., 2012b), and Mount Epomeo Green Tuff (MEGT, Y7; Wulf et al., 2004, 2007; Bourne et al., 2010; Tomlinson et al., 2014b).

Figures 15 and 16 show the TAS plot and detailed major element plots for these data, again providing a broad overview of the range of compositions present. Table 6 shows the matrix $\boldsymbol{A}$ based on multivariate normal statistics and Table 7 the matrix $\boldsymbol{B}$ based on KDE distributions. As with the other example applications, the conclusions are broadly similar using the two approaches. The consequences of these analyses are discussed from the point-of-view of the tephra lattice in Bronk Ramsey et al. (2014b).

Although there is little difference between the multivariate normal and KDE matrices, it is apparent from Figure 10 that the kernel density distribution does better represent the distribution of glass compositions. As both methods are easily applied, it seems most appropriate to use the KDE matrix if only one is used. However, by looking at both matrices it is possible to test how robust the conclusions are under different assumptions.

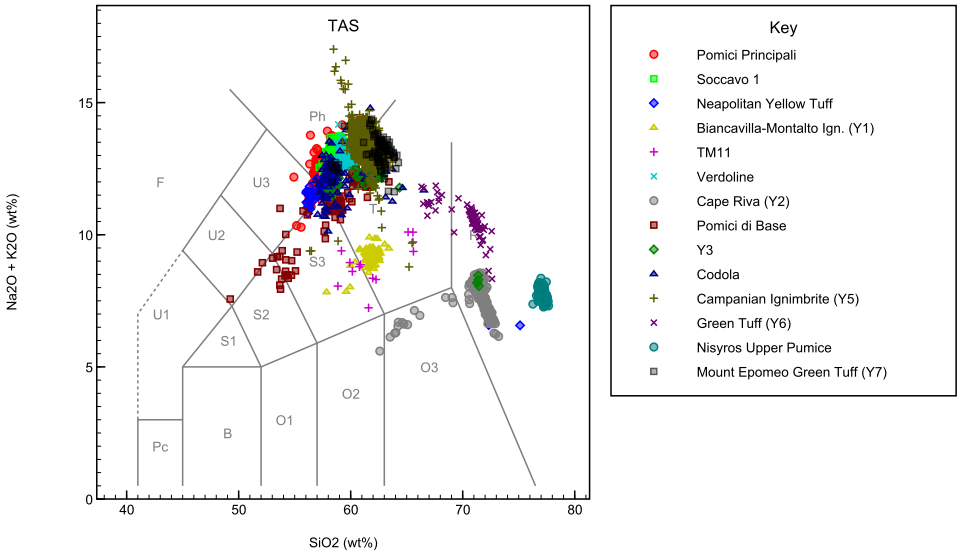

Fig. 15. TAS plot (normalised) for glass shard analyses for tephra/cryptotephra deposits from the Mediterranean region which are components of the RESET tephra lattice (Bronk Ramsey et al., 2014b).

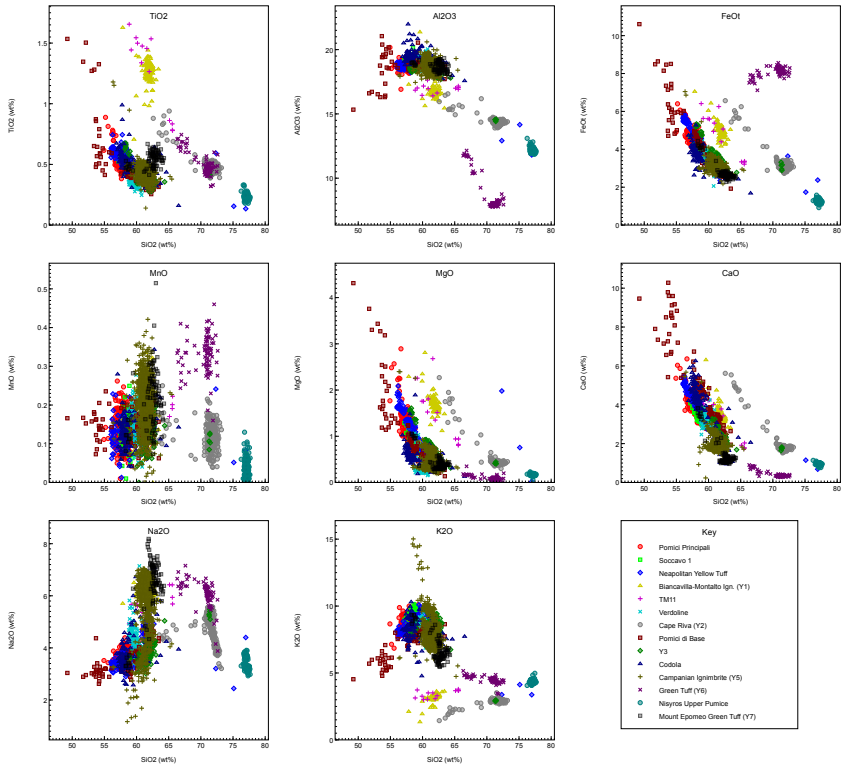

Fig. 16. Major element plots (normalised) for glass shard analyses for tephra/cryptotephra deposits from the Mediterranean region (c.f. Figure 15).

Datasets	A	B	C	D	E	F	G	H	I	J	K	L	M	N
A - Pomici Principali	1.000	**0.183**	**0.628**	0.000	0.000	0.000	0.000	0.001	0.026	0.019	0.000	0.000	0.000	0.004
B - Soccavo 1	**0.254**	1.000	**0.241**	0.000	0.000	0.000	0.000	0.000	0.019	**0.109**	0.000	0.000	0.000	0.003
C - Neapolitan Yellow Tuff	**0.078**	0.002	1.000	0.000	0.000	0.000	0.000	0.025	**0.063**	**0.166**	**0.051**	0.000	0.000	0.005
D - Biancavilla-Montalto Ign. (Y1)	0.000	0.000	0.000	1.000	0.007	0.000	0.000	0.000	0.000	0.000	0.000	0.000	0.000	0.000
E - TM11	0.000	0.000	0.000	0.000	1.000	0.000	0.000	0.000	0.000	0.000	0.000	0.000	0.000	0.000
F - Verdoline	0.000	0.000	0.004	0.000	0.000	1.000	0.000	0.021	0.000	0.037	0.002	0.000	0.000	0.001
G - Cape Riva (Y2)	0.000	0.000	0.000	0.000	0.000	0.000	1.000	0.000	0.001	0.000	0.000	0.000	0.000	0.000
H - Pomici di Base	0.000	0.000	0.000	0.000	0.000	0.001	0.000	1.000	0.000	**0.105**	0.000	0.000	0.000	0.000
I - Y3	0.001	0.000	**0.312**	0.000	0.000	0.000	**0.093**	0.047	1.000	0.028	0.036	0.000	0.000	0.002
J - Codola	0.000	0.000	0.017	0.000	0.000	0.000	0.000	0.002	0.011	1.000	0.029	0.000	0.000	0.005
K - Campanian Ignimbrite (Y5)	0.000	0.000	0.009	0.000	0.000	0.000	0.000	0.003	0.031	0.023	1.000	0.000	0.000	0.010
L - Green Tuff (Y6)	0.000	0.000	0.000	0.000	0.000	0.000	0.000	0.000	0.000	0.000	0.000	1.000	0.000	0.000
M - Nisyros Upper Pumice	0.000	0.000	0.000	0.000	0.000	0.000	0.000	0.000	0.000	0.000	0.000	0.000	1.000	0.000
N - Mount Epomeo Green Tuff (Y7)	0.031	0.003	**0.131**	0.000	0.000	0.000	0.000	0.007	0.039	0.032	0.014	0.000	0.000	1.000

Table 6. Matrix $\boldsymbol{A_{YX}}$ based on multivatiate normal probability distributions (SiO_2, TiO_2, Al_2O_3, FeOt, MnO, MgO, CaO, Na_2O, K_2O) for glass from tephras from the Mediterranean region which are important in the RESET tephra lattice.

Datasets	A	B	C	D	E	F	G	H	I	J	K	L	M	N
A - Pomici Principali	1.000	**0.195**	**0.459**	0.000	0.000	0.000	0.000	0.002	0.031	0.018	0.000	0.000	0.000	0.022
B - Soccavo 1	**0.253**	1.000	**0.169**	0.000	0.000	0.001	0.000	0.000	0.034	**0.105**	0.000	0.000	0.000	0.019
C - Neapolitan Yellow Tuff	**0.062**	0.006	1.000	0.000	0.000	0.000	0.000	0.042	**0.093**	**0.135**	0.021	0.000	0.000	0.019
D - Biancavilla-Montalto Ign. (Y1)	0.000	0.000	0.000	1.000	0.017	0.000	0.000	0.000	0.000	0.000	0.000	0.000	0.000	0.000
E - TM11	0.000	0.000	0.000	0.000	1.000	0.000	0.000	0.000	0.000	0.000	0.000	0.000	0.000	0.000
F - Verdoline	0.000	0.000	0.006	0.000	0.000	1.000	0.000	0.037	0.001	0.035	0.002	0.000	0.000	0.001
G - Cape Riva (Y2)	0.000	0.000	0.000	0.000	0.000	0.000	1.000	0.000	0.006	0.000	0.000	0.000	0.000	0.000
H - Pomici di Base	0.000	0.000	0.000	0.000	0.000	0.002	0.000	1.000	0.000	**0.072**	0.000	0.000	0.000	0.000
I - Y3	0.001	0.000	**0.244**	0.000	0.000	0.000	**0.122**	**0.081**	1.000	0.023	0.018	0.000	0.000	0.005
J - Codola	0.000	0.000	0.017	0.000	0.000	0.000	0.000	0.003	0.020	1.000	0.013	0.000	0.000	0.005
K - Campanian Ignimbrite (Y5)	0.000	0.000	0.013	0.000	0.000	0.000	0.000	0.006	0.047	0.025	1.000	0.000	0.000	0.009
L - Green Tuff (Y6)	0.000	0.000	0.000	0.000	0.000	0.000	0.000	0.000	0.000	0.000	0.000	1.000	0.000	0.000
M - Nisyros Upper Pumice	0.000	0.000	0.000	0.000	0.000	0.000	0.000	0.000	0.000	0.000	0.000	0.000	1.000	0.000
N - Mount Epomeo Green Tuff (Y7)	0.038	0.006	**0.103**	0.000	0.000	0.000	0.000	0.010	0.030	0.030	0.007	0.000	0.000	1.000

Table 7. Matrix $\boldsymbol{B_{YX}}$ based on KDE probability distributions (SiO_2, TiO_2, Al_2O_3, FeOt, MnO, MgO, CaO, Na_2O, K_2O) for glass from tephras from the Mediterranean region which are important in the RESET tephra lattice.

6 Conclusions

Data *per se* are only valuable if they can be used. As datasets become larger and more complex, retaining usability becomes a larger challenge. Tephra studies do generate large quantities of data, and the RESET database has been designed to ensure that these datasets remain useful for researchers across many different projects. The aim of this database is to make the data useful, not only by making navigation of the database easy, but also by providing tools for visualisation and statistical analysis of the data which are directly linked with the database itself. These functions do not require the installation of any special software and so allow anyone to explore the data freely.

There are more things that could be done to the database to develop it further: in particular, as people use the database more, it is expected that new types of database query might be added. However, the framework used to generate the database is very flexible and so should be relatively easy to modify. The other import aspect of a working will be the management of additions to the database from new publications.

This database has also already spawned other tools. In particular, the INTIMATE database and chronological integration tool (Bronk Ramsey et al., 2014a) grew directly from the framework of the RESET database. Likewise the mapping elements within OxCal (Bronk Ramsey and Lee, 2013) were a byproduct of the RESET mapping functions. Together these provide a whole group of tools that can help in Quaternary research.

7 Acknowledgements

The research and developments behind this paper were conducted in support of a project funded by the Natural Environment Research Council (NERC) on the Response of Humans to Abrupt Environmental Transitions (RESET; NE/E015670/1). The authors would like to express their thanks to NERC for funding and to all the other members of the RESET team, who contributed to this database. However, this research would not have been possible without all of the work done by previous researchers in this area. Their published data forms an important element of this database. Collection of data was also helped enormously by the compilation of tephra conducted for the NERC QUEST project, and by Felix Riede's compilation of sites where the Laacher See Tephra has been found.

References

Aitchison, J., Lauder, I., 1985. Kernel density estimation for compositional data. Applied statistics, 129–137.

Albert, P. G., Tomlinson, E. L., Smith, V. C., Roberto, D. A., Todman, A., Rosi, M., Marani, M., Muller, W., Menzies, M. A., 2012. Marine-continental tephra correlations: Volcanic glass geochemistry from the Marsili Basin and the Aeolian Islands, Southern Tyrrhenian Sea, Italy. Journal of Volcanology and Geothermal Research 229-230, 74–94.

Andrews, J. T., Geirsdóttir, A., Hardardóttir, J., Principato, S., Grönvold, K., Kristjansdóttir, G. B., Helgadóttir, G., Drexler, J., Sveinbjörnsdóttir, A., 2002. Distribution, sediment magnetism and geochemistry of the Saksunarvatn (10 180 60 cal. yr BP) tephra in marine, lake, and terrestrial sediments, northwest Iceland. Journal of Quaternary Science 17 (8), 731–745.

Baxter, M. J., Beardah, C., Wright, R., 1997. Some archaeological applications of kernel density estimates. Journal of Archaeological Science 24 (4), 347–354.

Birks, H. H., Gulliksen, S., Haflidason, H., Mangerud, J., Possnert, G., 1996. New Radiocarbon Dates for the Vedde Ash and the Saksunarvatn Ash from Western Norway. Quaternary Research 45 (2), 119–127.

Björck, J., Wastegård, S., 1999. Climate oscillations and tephrochronology in eastern middle Sweden during the last glacial-interglacial transition. Journal of Quaternary Science 14 (5), 399–410.

Blockley, S. P. E., Lane, C. S., Lotter, A. F., Pollard, A. M., 2007. Evidence for the presence of the Vedde Ash in Central Europe. Quaternary Science Reviews 26 (25-28), 3030–3036.

Bourne, A. J., Lowe, J. J., Trincardi, F., Asioli, A., Blockley, S. P. E., Wulf, S., Matthews, I. P., Piva, A., Vigliotti, L., 2010. Distal tephra record for the last ca 105,000 years from core PRAD 1-2 in the central Adriatic Sea: implications for marine tephrostratigraphy. Quaternary Science Reviews 29 (23-24), 3079–3094.

Bowman, A. W., Azzalini, A., 1997. Applied Smoothing Techniques for Data Analysis. Oxford University Press, London.

Bramham-Law, C. W. F., Theuerkauf, M., Lane, C. S., Mangerud, J., 2013. New findings regarding the Saksunarvatn Ash in Germany. Journal of Quaternary Science 28 (3), 248–257.

Bronk Ramsey, C., Albert, P., Blockley, S., Hardiman, M., Lane, C., Macleod, A., Matthews, I. P., Muscheler, R., Palmer, A., Staff, R. A., 2014a. Integrating timescales with time-transfer functions: a practical approach for an INTIMATE database. Quaternary Science Reviews submitted.

Bronk Ramsey, C., Albert, P., Hardiman, M., Housley, R. A., Lane, C. S., Lee, S., Matthews, I. P., Smith, V. C., Lowe, J., 2014b. Improved age estimates for important Late Quaternary European tephra horizons in the RESET lattice. Quaternary Science Reviews submitted.

Bronk Ramsey, C., Lee, S., 2013. Recent and Planned Developments of the

Program OxCal. Radiocarbon 55 (2-3), 720–730.

Davies, S. M., Hoek, W. Z., Bohncke, S. J. P., Lowe, J. J., O'Donnell, S. P., Turney, C. S. M., 2005. Detection of Lateglacial distal tephra layers in the Netherlands. Boreas 34 (2), 123–135.

Davies, S. M., Turney, C. S. M., Lowe, J. J., 2001. Identification and significance of a visible, basalt-rich Vedde Ash layer in a Late-glacial sequence on the Isle of Skye, Inner Hebrides, Scotland. Journal of Quaternary Science 16 (2), 99–104.

Davies, S. M., Wastegård, S., Wohlfarth, B., 2003. Extending the limits of the Borrobol Tephra to Scandinavia and detection of new early Holocene tephras. Quaternary Research 59 (3), 345–352.

Douka, K., Jacobs, Z., Lane, C., Grun, R., Farr, L., Hunt, C., Inglis, R. H., Reynolds, T., Albert, P., Aubert, M., Cullen, V., Hill, E., Kinsley, L., Roberts, R. G., Tomlinson, E. L., Wulf, S., Barker, G., 2014. The chronostratigraphy of the Haua Fteah cave (Cyrenaica, northeast Libya). Journal of Human Evolution 66, 39–63.

Dugmore, A. J., Newton, A. J., 1997. Holocene tephra layers in the Faroe Islands. Frodskaparrit 45, 141–154.

Finsinger, W., Belis, C., Blockley, S. P. E., Eicher, U., Leuenberger, M., Lotter, A. F., Ammann, B., 2008. Temporal patterns in lacustrine stable isotopes as evidence for climate change during the late glacial in the Southern European Alps. Journal of Paleolimnology 40 (3), 885–895.

Housley, R. A., Lane, C. S., Cullen, V. L., Weber, M. J., Riede, F., Gamble, C. S., Brock, F., 2012. Icelandic volcanic ash from the Late-glacial open-air archaeological site of Ahrenshoft LA 58 D, North Germany. Journal of Archaeological Science 39, 708–716.

Housley, R. A., MacLeod, A., Nalepka, D., Jurochnik, A., Masojc, M., Davies, L., Lincoln, P. C., Ramsey, C. B., Gamble, C. S., Lowe, J. J., 2013. Tephrostratigraphy of a Lateglacial lake sediment sequence at Wegliny, southwest Poland. Quaternary Science Reviews 77, 4–18.

Jochum, K. P., Stoll, B., Herwig, K., Willbold, M., Hofmann, A. W., Amini, M., Aarburg, S., Abouchami, W., Hellebrand, E., Mocek, B., Raczek, I., Stracke, A., Alard, O., Bouman, C., Becker, S., Dßcking, M., Brätz, H., Klemd, R., de Bruin, D., Canil, D., Cornell, D., de Hoog, C.-J., Dalpé, C., Danyushevsky, L., Eisenhauer, A., Gao, Y., Snow, J. E., Groschopf, N., Gßnther, D., Latkoczy, C., Guillong, M., Hauri, E. H., Höfer, H. E., Lahaye, Y., Horz, K., Jacob, D. E., Kasemann, S. A., Kent, A. J. R., Ludwig, T., Zack, T., Mason, P. R. D., Meixner, A., Rosner, M., Misawa, K., Nash, B. P., Pfänder, J., Premo, W. R., Sun, W. D., Tiepolo, M., Vannucci, R., Vennemann, T., Wayne, D., Woodhead, J. D., 2006. MPI-DING reference glasses for in situ microanalysis: New reference values for element concentrations and isotope ratios. Geochemistry, Geophysics, Geosystems 7 (2). URL `http://dx.doi.org/10.1029/2005GC001060`

Kwiecien, O., Arz, H. W., Lamy, F., Wulf, S., Bahr, A., Röhl, U., Haug, G. H., 2008. Estimated reservoir ages of the Black Sea since the Last Glacial.

Radiocarbon 50 (1), 99–118.
Lane, C. S., Andric, M., Cullen, V. L., Blockley, S. P. E., 2011a. The occurrence of distal Icelandic and Italian tephra in the Lateglacial of Lake Bled, Slovenia. Quaternary Science Reviews 30 (9-10), 1013–1018.
Lane, C. S., Blockley, S. P. E., Bronk Ramsey, C., Lotter, A. F., 2011b. Tephrochronology and absolute centennial scale synchronisation of European and Greenland records for the last glacial to interglacial transition: A case study of Soppensee and NGRIP. Quaternary International 246 (1-2), 145–156.
Lane, C. S., Blockley, S. P. E., Lotter, A. F., Finsinger, W., Filippi, M. L., Matthews, I. P., 2011c. A regional tephrostratigraphic framework for central and southern European climate archives during the Last Glacial to Interglacial transition: comparisons north and south of the Alps. Quaternary Science Reviews 36, 50–58.
Lane, C. S., Blockley, S. P. E., Mangerud, J., Smith, V. C., Lohne, O. S., Tomlinson, E. L., Matthews, I. P., Lotter, A. F., 2012a. Was the 12.1 ka Icelandic Vedde Ash one of a kind? Quaternary Science Reviews 33, 87–99.
Lane, C. S., Klerk, D. P., Cullen, V. L., 2012b. A tephrochronology for the Lateglacial palynological record of the Endinger Bruch (Vorpommern, north-east Germany). Journal of Quaternary Science 27 (2), 141–149.
Le Maitre, R. W. (Ed.), 2002. Igneous rocks: a classification and glossary of terms : recommendations of the International Union of Geological Sciences, Subcommission on the Systematics of Igneous Rocks. Cambridge University Press.
Lind, E. M., Wastegård, S., 2011. Tephra horizons contemporary with short early Holocene climate fluctuations: New results from the Faroe Islands. Quaternary International 246 (1-2), 157–167.
Lowe, J. J., Blockley, S. P. E., Trincardi, F., Asioli, A., Cattaneo, A., Matthews, I. P., Pollard, A. M., Wulf, S., 2007. Age modelling of late Quaternary marine sequences in the Adriatic: Towards improved precision and accuracy using volcanic event stratigraphy. Continental Shelf Research, 27 (3-4), 560–582.
Lowe, J. J., Turney, C. S. M., 1997. Vedde Ash layer discovered in a small lake basin on the Scottish mainland. Journal of the Geological Society, London 154 (4), 605–612.
Magny, M., de Beaulieu, J.-L., Drescher-Schneider, R., Vannière, B., Walter-Simonnet, A.-V., Millet, L., Bossuet, G., Peyron, O., 2006. Climatic oscillations in central Italy during the Last Glacial-Holocene transition: the record from Lake Accesa. Journal of Quaternary Science 21 (4), 311–320.
Margari, V., Pyle, D. M., Bryant, C., Gibbard, P. L., 2007. Mediterranean tephra stratigraphy revisited: Results from a long terrestrial sequence on Lesvos Island, Greece. Journal of Volcanology and Geothermal Research 163 (1-4), 34–54.
Matthews, I. P., Birks, H. H., Bourne, A. J., Brooks, S. J., Lowe, J. J., MacLeod, A., Pyne-O'Donnell, S. D. F., 2011. New age estimates and

climatostratigraphic correlations for the Borrobol and Penifiler Tephras: evidence from Abernethy Forest, Scotland. Journal of Quaternary Science 26 (3), 247–252.

Morley, M. W., Woodward, J. C., 2011. The Campanian Ignimbrite (Y5) tephra at Crvena Stijena Rockshelter, Montenegro. Quaternary Research 75, 683–696.

Pilcher, J., Bradley, R., Francus, P., Anderson, L., 2005. A Holocene tephra record from the Lofoten Islands, Arctic Norway. Boreas 34 (2), 136–0.

Pyle, D. M., Ricketts, G. D., Margari, V., van Andel, T. H., Sinitsyn, A. A., Praslov, N. D., Lisitsyn, S., 2006. Wide dispersal and deposition of distal tephra during the Pleistocene Campanian Ignimbrite/Y5 eruption, Italy. Quaternary Science Reviews 25 (21-22), 2713–2728.

Pyne-O'Donnell, S. D. F., 2007. Three new distal tephras in sediments spanning the Last Glacial-Interglacial Transition in Scotland. Journal of Quaternary Science 22 (6), 559–570.

Pyne-O'Donnell, S. D. F., Blockley, S. P. E., Turney, C. S. M., Lowe, J. J., 2008. Distal volcanic ash layers in the Lateglacial Interstadial (GI-1): problems of stratigraphic discrimination. Quaternary Science Reviews 27 (1-2), 72–84.

Ranner, P. H., Allen, J. R. M., Huntley, B., 2005. A new early Holocene cryptotephra from northwest Scotland. Journal of Quaternary Science 20 (3), 201–208.

Riede, F., Bazely, O., Newton, A. J., Lane, C. S., 2011. A Laacher See-eruption supplement to Tephrabase: Investigating distal tephra fallout dynamics. Quaternary International 246 (1-2), 134–144.

Riede, F., Wheeler, J. M., 2009. Testing the "Laacher See hypothesis": tephra as dental abrasive. Journal of Archaeological Science 36 (10), 2384–2391.

Santos, J., Munita, C., Valério, M., Vergne, C., Oliveira, P., 2006. Determination of trace elements in archaeological ceramics and application of Kernel Density Estimates: Implications for the definition of production locations. Journal of radioanalytical and nuclear chemistry 269 (2), 441–445.

Schoning, K., Klingberg, F., Wastegård, S., 2001. Marine conditions in central Sweden during the early Preboreal as inferred from a stable oxygen isotope gradient. Journal of Quaternary Science 16 (8), 785–794.

Scott, D. W., 1992. Multivariate Density Estimation: Theory, Practice, and Visualization. Wiley, New York.

Seymour, K. S. K. S., Christanis, K., 1995. Correlation of a Tephra Layer in Western Greece with a Late Pleistocene Eruption in the Campanian Province of Italy. Quaternary Research 43 (1), 46–54.

Smith, V. C., Isaia, R., Pearce, N. J. G., 2011. Tephrostratigraphy and glass compositions of post-15 kyr Campi Flegrei eruptions: implications for eruption history and chronostratigraphic markers. Quaternary Science Reviews 30 (25-26), 3638–3660.

Tomlinson, E., Smith, V., Albert, P., Aydar, E., Civetta, L., Cioni, R., Çubukçu, E., Gertisser, R., Isaia, R., Menzies, M., Orsi, G., Rosi, M.,

Zanchetta, G., 2014a. Determining the source of <100 ka tephra layers in the central and eastern mediterranean. Quaternary Science Reviews this volume.

Tomlinson, E. L., Albert, P. G., Wulf, S., Brown, R., Smith, V. C., Keller, J., Orsi, G., Bourne, A. J., Menzies, M. A., 2014b. Age and geochemistry of tephra layers from Ischia, Italy: constraints from proximal-distal correlations with Lago Grande di Monticchio. Journal of volcanology and Geothermal Research in press.

Tomlinson, E. L., Arienzo, I., Civetta, L., Wulf, S., Smith, V. C., Hardiman, M., Lane, C. S., Carandente, A., Orsi, G., Rosi, M., Muller, W., Menzies, M. A., 2012a. Geochemistry of the Phlegraean Fields (Italy) proximal sources for major Mediterranean tephras: Implications for the dispersal of Plinian and co-ignimbritic components of explosive eruptions. Geochimica et Cosmochimica Acta 93, 102–128.

Tomlinson, E. L., Kinvig, H. S., Smith, V. C., Blundy, J. D., Gottsmann, J., Muller, W., Menzies, M. A., 2012b. The Upper and Lower Nisyros Pumices: Revisions to the Mediterranean tephrostratigraphic record based on micron-beam glass geochemistry. Journal of Volcanology and Geothermal Research 243-244, 69–80.

Turney, C. S. M., Burg, V. D. K., Wastegård, S., Davies, S. M., Whitehouse, N. J., Pilcher, J. R., Callaghan, C., 2006. North European last glacial-interglacial transition (LGIT; 15-9 ka) tephrochronology: extended limits and new events. Journal of Quaternary Science 21 (4), 335–345.

Turney, C. S. M., Harkness, D. D., Lowe, J. J., 1997. The use of microtephra horizons to correlate Late-glacial lake sediment successions in Scotland. Journal of Quaternary Science 12 (6), 525–531.

Turney, C. S. M., Lowe, J. J., Wastegård, S., Cooper, R., Roberts, S. J., 2001. The development of a tephrochronological framework for the last glacial-Holocene transition in NW Europe. In: Juvigne, E. H., Raynal, J.-P. (Eds.), Tephras: Chronology, Archaeology. Vol. 1. Dossiers de l'Archéo-Logis, Haute-Loire, pp. 101–109.

Vogel, H., Zanchetta, G., Sulpizio, R., Wagner, B., Nowaczyk, N., 2009. A tephrostratigraphic record for the last glacial-interglacial cycle from Lake Ohrid, Albania and Macedonia. Journal of Quaternary Science 25 (3), 320–338.

Wastegård, S., Bjorck, S., Grauert, M., Hannon, G. E., 2001. The Mjauvotn tephra and other Holocene tephra horizons from the Faroe Islands: a link between the Icelandic source region, the Nordic Seas, and the European continent. The Holocene 11 (1), 101–109.

Wastegård, S., Björck, S., Possnert, G., Wohlfarth, B., 1998. Evidence for the occurrence of Vedde Ash in Sweden: radiocarbon and calendar age estimates. Journal of Quaternary Science 13 (3), 271–274.

Wastegård, S., Wohlfarth, B., Subetto, D. A., Sapelko, T. V., 2000. Extending the known distribution of the Younger Dryas Vedde Ash into northwestern Russia. Journal of Quaternary Science 15 (6), 581–586.

Weller, J. N., Martin, A. J., Connor, C. B., Connor, L., Karakhanian, A., 2006. Modelling the spatial distribution of volcanoes: an example from Armenia. Statistics in Volcanology, Special Publications of IAVCEI 1, 77–87.

Wulf, S., Brauer, A., Mingram, J., Zolitschka, B., Negendank, J. F. W., 2007. Distal tephras in the sediments of Monticchio maar lakes. In: Principe, C. (Ed.), Geologia del Monte Vulture. Bollettino della Società Geologica Italiana. Bollettino della Società Geologica Italiana, pp. 105–122.

Wulf, S., Kraml, M., Brauer, A., Keller, J., Negendank, J. F. W., 2004. Tephrochronology of the 100 ka lacustrine sediment record of Lago Grande di Monticchio (southern Italy). Quaternary International 122 (1), 7–30.

Wulf, S., Kraml, M., Kuhn, T., Schwarz, M., Inthorn, M., Keller, J., Kuscu, I., Halbach, P., 2002. Marine tephra from the Cape Riva eruption (22 ka) of Santorini in the Sea of Marmara. Marine Geology 183 (1-4), 131–141.

Zhang, X., King, M. L., Hyndman, R. J., 2006. A Bayesian approach to bandwidth selection for multivariate kernel density estimation. Computational Statistics & Data Analysis 50 (11), 3009–3031.

A Supplementary Information

A.1 Glass-shard major element data (non-normalised) for the Soppensee case study

Layer	SiO_2	TiO_2	Al_2O_3	FeOt*	MnO	MgO	CaO	Na_2O	K_2O	total
Sop_T4.74	67.12	0.46	15.38	1.96	0.21	0.22	0.70	5.37	5.82	97.24
Sop_T4.74	65.41	0.40	15.60	1.84	0.19	0.22	0.86	5.14	5.58	95.23
Sop_T4.74	67.62	0.46	15.39	1.82	0.24	0.25	0.71	5.16	5.88	97.52
Sop_T4.74	65.13	0.08	20.05	0.65	0.00	0.04	2.16	7.82	3.50	99.44
Sop_T4.74	66.94	0.27	17.35	1.01	0.11	0.14	0.76	6.15	6.44	99.16
Sop_T4.74	66.27	0.38	15.67	1.74	0.22	0.21	0.88	5.49	5.37	96.23
Sop_T4.74	66.67	0.33	16.44	1.47	0.17	0.24	0.99	6.11	5.59	98.02
Sop_T4.74	67.58	0.43	15.67	1.87	0.25	0.22	0.75	5.66	5.72	98.14
Sop_T4.74	64.86	0.04	20.25	0.48	0.00	0.02	2.23	8.10	3.37	99.36
Sop_T4.74	66.07	0.13	18.31	0.70	0.02	0.06	0.84	6.58	6.28	98.98
Sop_T4.74	68.67	0.42	14.86	1.97	0.27	0.22	0.64	5.45	5.47	97.94
Sop_T4.74	67.27	0.24	17.55	1.12	0.17	0.11	1.16	6.84	4.96	99.40
Sop_T4.74	65.44	0.18	18.52	0.79	0.11	0.06	1.23	6.83	5.27	98.42
Sop_T4.74	66.53	0.29	16.49	1.35	0.21	0.15	0.70	5.77	6.03	97.52
Sop_T4.74	65.52	0.41	15.54	1.59	0.22	0.21	0.88	5.24	5.34	94.95
Sop_T4.74	65.33	0.35	16.35	1.42	0.17	0.20	1.02	5.84	5.42	96.09
Sop_T4.74	64.59	0.06	20.21	0.53	0.00	0.02	2.07	7.64	4.03	99.16
Sop_T4.74	67.17	0.44	15.87	1.80	0.20	0.25	0.74	5.63	5.79	97.89
Sop_T4.74	66.70	0.37	16.91	1.58	0.19	0.19	1.34	6.17	4.94	98.39
Sop_T4.74	65.50	0.22	18.61	1.25	0.14	0.12	1.92	6.72	4.34	98.82
Sop_T4.74	65.71	0.18	19.48	0.83	0.04	0.05	2.05	7.62	3.66	99.63
Sop_T4.74	66.81	0.48	14.82	2.15	0.30	0.24	0.65	5.09	5.89	96.43
Sop_T4.74	66.66	0.18	18.23	0.87	0.03	0.05	1.01	6.85	5.50	99.37
Sop_T4.74	65.44	0.10	19.01	0.62	0.09	0.02	0.99	7.08	5.56	98.92
Sop_T5.19	75.19	0.31	12.36	2.55	0.08	0.25	1.64	3.84	2.53	98.74
Sop_T5.19	73.98	0.29	12.39	2.43	0.07	0.24	1.48	3.89	2.56	97.33
Sop_T5.19	75.76	0.31	12.48	2.69	0.00	0.19	1.59	3.89	2.53	99.45
Sop_T5.19	72.71	0.31	11.85	2.37	0.00	0.24	1.67	4.04	2.38	95.70
Sop_T5.19	73.00	0.26	11.77	2.46	0.06	0.24	1.60	4.08	2.39	95.98
Sop_T5.62	71.08	0.31	13.57	3.77	0.12	0.23	1.35	4.47	3.60	98.49
Sop_T5.62	69.50	0.28	13.36	3.54	0.10	0.21	1.19	4.60	3.23	96.01
Sop_T5.62	71.08	0.29	13.76	3.66	0.19	0.21	1.26	4.81	3.38	98.65
Sop_T5.62	71.55	0.28	13.70	3.71	0.19	0.21	1.30	4.49	3.52	98.95
Sop_T5.62	70.10	0.26	13.35	3.64	0.13	0.21	1.28	4.89	3.47	97.33
Sop_T5.62	68.72	0.27	12.73	3.53	0.13	0.18	1.24	4.93	3.35	95.06
Sop_T5.62	72.46	0.29	13.53	3.87	0.11	0.21	1.30	5.36	3.41	100.52
Sop_T5.62	72.44	0.30	13.72	3.82	0.22	0.20	1.27	5.07	3.50	100.54
Sop_T5.95	57.70	0.23	22.79	1.64	0.21	0.04	0.91	10.74	5.56	100.25
Sop_T5.95	57.38	0.24	22.80	1.72	0.29	0.04	0.90	10.43	5.61	99.84
Sop_T5.95	57.47	0.21	22.76	1.93	0.25	0.05	0.79	10.64	5.62	100.16
Sop_T5.95	57.20	0.20	23.01	1.81	0.28	0.08	0.74	10.88	5.64	100.22
Sop_T5.95	57.15	0.26	23.05	1.75	0.36	0.07	0.88	10.35	5.52	99.88
Sop_T5.95	57.95	0.19	22.90	1.71	0.31	0.05	0.91	10.29	5.71	100.49
Sop_T5.95	57.41	0.21	23.12	1.73	0.36	0.06	0.90	10.73	5.66	100.59
Sop_T5.95	56.04	0.17	22.56	1.86	0.39	0.08	0.88	9.86	5.38	97.66
Sop_T5.95	59.26	0.24	22.33	1.74	0.36	0.03	1.09	9.81	5.32	100.44
Sop_T5.95	58.33	0.21	22.88	1.37	0.22	0.03	1.05	10.31	4.79	99.60
Sop_T5.95	55.88	0.23	22.00	1.72	0.23	0.13	1.25	10.23	4.99	97.13
Sop_T5.95	57.25	0.19	23.19	1.65	0.35	0.04	0.74	11.30	5.19	100.34
Sop_T5.95	57.50	0.20	22.62	1.91	0.30	0.06	0.87	10.54	5.58	100.03
Sop_T5.95	57.89	0.26	22.51	1.77	0.33	0.04	0.86	10.41	5.62	100.16

Layer	SiO_2	TiO_2	Al_2O_3	FeOt*	MnO	MgO	CaO	Na_2O	K_2O	total
Sop_T5.95	57.51	0.22	22.84	1.75	0.33	0.10	0.87	10.81	5.65	100.51
Sop_T5.95	56.79	0.22	23.41	1.70	0.28	0.05	0.74	10.74	5.22	99.64
Sop_T5.95	57.55	0.21	23.01	1.68	0.23	0.07	0.85	10.71	5.54	100.27
Sop_T5.95	55.09	0.18	22.54	1.69	0.26	0.03	0.95	9.95	5.41	96.61
Sop_T5.95	57.59	0.21	22.75	1.95	0.25	0.07	0.89	10.81	5.69	100.62
Sop_T5.95	57.38	0.19	22.40	1.79	0.24	0.05	0.82	11.10	5.34	99.74
Sop_T5.95	57.87	0.18	23.13	1.71	0.32	0.10	0.88	10.56	5.56	100.77
Sop_T5.95	58.23	0.22	23.07	1.89	0.22	0.03	0.99	10.43	5.39	100.92
Sop_T5.95	59.54	0.08	22.62	1.17	0.25	0.03	1.05	9.94	4.99	99.96
Sop_T5.95	57.74	0.21	22.96	1.64	0.29	0.07	0.92	10.31	5.53	100.23
Sop_T5.95	57.92	0.20	22.71	1.77	0.32	0.05	0.86	10.34	5.68	100.26
Sop_T5.95	57.70	0.27	23.60	1.79	0.31	0.06	0.87	10.34	5.51	100.92
Sop_T5.95	57.66	0.18	22.85	1.71	0.28	0.04	1.04	10.17	5.66	100.01
Sop_T5.95	57.51	0.16	23.34	1.92	0.24	0.06	0.72	11.03	5.40	100.78
Sop_T5.95	55.82	0.19	22.00	1.68	0.29	0.08	0.86	10.14	5.56	97.07
Sop_T5.95	57.58	0.18	22.81	1.42	0.28	0.08	0.70	10.32	5.28	99.20
Sop_T5.95	57.89	0.24	22.65	1.80	0.18	0.05	0.79	10.26	5.59	99.87
Sop_T5.95	59.85	0.10	21.76	1.00	0.18	0.05	1.02	8.77	6.21	99.22
Sop_T5.95	57.72	0.24	22.96	1.82	0.28	0.06	0.89	9.84	5.50	99.80
Sop_T5.95	57.27	0.23	22.80	1.71	0.24	0.03	0.87	10.42	5.48	99.55
Sop_T5.95	57.80	0.18	22.52	1.80	0.32	0.06	0.84	10.25	5.54	99.73

* total iron oxides